LA-13753-T
Thesis

Fidelity of a Finite Element Model for Longitudinal Wave Propagation in Thick Cylindrical Wave Guides

Los Alamos
NATIONAL LABORATORY

Los Alamos National Laboratory is operated by the University of California for the United States Department of Energy under contract W-7405-ENG-36.

This thesis was accepted by the Department of Mechanical Engineering, Colorado State University, Fort Collins, Colorado, in partial fulfillment of the requirements for the degree of Master of Science. The text and illustrations are the independent work of the author and only the front matter has been edited by the CIC-1 Writing and Editing Staff to conform with Department of Energy and Los Alamos National Laboratory publication policies.

An Affirmative Action/Equal Opportunity Employer

LA-13753-T
Thesis

Issued: September 2000

Fidelity of a Finite Element Model for Longitudinal Wave Propagation in Thick Cylindrical Wave Guides

*Anthony D. Puckett**

**Graduate Research Assistant at Los Alamos National Laboratory. Engineering Analysis Group (ESA-EA), in the Engineering Sciences and Applications Division.*

Los Alamos
NATIONAL LABORATORY
Los Alamos, New Mexico 87545

ACKNOWLEDGEMENTS:

The funding for this research was provided by the Accelerated Strategic Computing Initiative (ASCI) through Los Alamos National Laboratory. The Engineering Analysis Group of the Engineering Science Applications Division at Los Alamos National Laboratory provided computer resources and additional support.

TABLE OF CONTENTS

NOMENCLATURE

E	Young's modulus
K_i	wavenumber (1/unit length), i = mode number
T	period of wave
V(x)	continuous data set
V[x]	discrete data set
a	radius
c_0	velocity of longitudinal waves in an infinitesimally thin bar $= \sqrt{E/\rho}$
c_d	velocity of dilatational waves in an unbounded medium $= \sqrt{(\lambda + 2\mu)/\rho}$
c_g	group velocity $= d\omega/dk$
c_p	phase velocity
c_R	velocity of Rayleigh waves
c_s	velocity of shear (transverse) waves in an unbounded medium $= \sqrt{\mu/\rho}$
f	frequency (Hz) $f = 1/T = \omega/2\pi = c_p/\Lambda$
k	wavenumber (radians/unit length) $= \omega/c_p$
Λ	wavelength
ε_x	strain, x direction
λ, μ	Lamé constants
ρ	density
τ_x	stress, x direction
ω	frequency (rad/s)

FIDELITY OF A FINITE ELEMENT MODEL OF LONGITUDINAL WAVE PROPAGATION IN THICK CYLINDRICAL WAVE GUIDES

Anthony David Puckett

ABSTRACT

The ability to model wave propagation in circular cylindrical bars of finite length numerically or analytically has many applications. In this thesis the capability of an explicit finite element method to model longitudinal waves in cylindrical rods with circular cross-sections is explored. Dispersion curves for the first four modes are compared to the analytical solution to determine the accuracy of various element sizes and time steps. Values for the time step and element size are determined that retain accuracy while minimizing computational time. The modeling parameters are validated by calculating a signal propagated with a broadband input force. Limitations on the applicability are considered along with modeling parameters that should be applicable to more general geometries.

1. INTRODUCTION

For the last half of the 20th century there was considerable interest in modeling longitudinal wave propagation in semi-infinite and finite bars with circular cross-sections. The problem can be solved analytically or numerically, and often it is useful to compare experimental results with these analytical and numerical results. However, for even simple axially symmetric problems, analytical solutions can be very complex mathematically, and numerical models can require extensive computer resources.

Analytically, the main challenge is the additional complexity associated with the boundary conditions of another surface (the end of the bar). A finite bar adds yet another surface and even more analytical complexity. Alternatively, the problem can be solved numerically using the finite element method. However, because of the need for spatial and time resolution, numerical solutions can become very computationally demanding, requiring large amounts of computer memory and disk resources as well as processor time. In particular, as higher frequency components are added, the increases in computational demands increase nonlinearly.

It would be very useful to know the compromises between the different approaches and when a particular solution technique is better for certain applications. In order to know if a finite element solution is more appropriate for an application, parameters must be determined so that accuracy is maintained while computational costs are minimized. The objective of this work is to identify these parameters and expand the fundamental understanding of the limits of numerically modeling longitudinal wave propa-

gation at high frequencies. This thesis establishes some initial guidelines for numerically modeling of wave propagation using the finite element method. Although these guidelines were developed using the simple cylindrical geometry, the intent is to provide design tools that will be valid for other geometries where analytical verification is not possible. Over the last century however, extensive research has been performed on the analytical solution to these problems.

The propagation of elastic waves in solids was studied extensively throughout the 19^{th} and 20^{th} centuries. In particular, the propagation of elastic waves in circular cross-sectional rods has been considered since the end of the 19^{th} century. The foundational contribution for wave motion in a bar of circular cross-section was by Pochhammer (1876) and later independently by Chree (1889).

Pochhammer derived the solution for three-dimensional wave propagation in infinite rods with a circular cross-section. The solution described longitudinal wave propagation as well as torsional and flexural wave propagation and is known as the Pochhammer-Chree solution. On the subject of longitudinal wave propagation in rods with circular cross-sections, three main areas of interest evolved after Pochhammer. The first area of interest was a one-dimensional approximation to the three-dimensional equation. The second area of interest was the experimental and numerical study of the Pochhammer-Chree solution. The other notable research area was the development of a solution similar to the Pochhammer-Chree solution but for a semi-infinite or finite bar.

The focus of this work is on the finite bar, but considered from the numerical side. The Pochhammer-Chree solution was used to determine the accuracy of numerical results of this thesis. If modeling using finite elements is found to be accurate compared to the analytical Pochhammer-Chree solution, then the same parameters may provide guidance

to model other geometries accurately. However, in order to model a bar accurately, the correct model with the correct parameters must be used.

This thesis used a three-dimensional axisymmetric model, which is a three-dimensional model in cylindrical coordinates that assumes there is no angular dependence of the stresses and displacements. This model describes the longitudinal wave propagation. Since there is no angular dependence, the model is a two-dimensional model of a radial slice of a cylinder. The three-dimensional axisymmetric solution used a commercial finite element code, ABAQUS, by Hibbitt, Karlsson, and Sorenson Inc. It should be noted that the axisymmetric model is quite simple and represents the minimal configuration and computational demand for a problem of significance. However, the parameters determined from the results of this work should provide insight into more complex geometries.

The first portion of this thesis is concerned with determining the correct parameters for modeling wave propagation with finite elements. First, the modeling of single mode propagation and exploring the effects of mesh size and time step on the accuracy of the model is considered. These results are used to determine the mesh size and time step for all of the multi-mode models. The parameters are then validated by comparing dispersion curves created from the Pochhammer frequency equation to dispersion curves created from the results of the FEA.

Insights from this work have applications to several areas of research especially in the field of nondestructive evaluation (NDE). An established technique to determine the Young's and shear moduli is the measurement of the time delay between the arrival of the first and second modes in a thick cylindrical waveguide. This is a key method for determining the moduli for materials at high temperatures (Peterson, 1999). Typically

large diameter cylinders are used, so the wave speed approaches that in an unbound medium. However, in a number of practical applications a smaller diameter cylinder must be used. For these cases dispersion plays a dominant role, and simple one-dimensional theory cannot predict the material properties. In these cases an analytical or numerical solution is required to evaluate the results. The experiment can be modeled with finite elements and the correct parameters to correctly predict material properties.

Recent research has also considered the application of guided waves to pipeline inspection (Aristégui, Cawley, and Lowe, 1999), timber characterization (Peterson, 1998), and other applications in non-destructive testing. In these and other cases the wave propagation problem needs to be modeled. The parameters from this thesis were explored using a circular cylindrical bar, however the parameters should be applicable to many different and more complex geometries.

This background then leads to the question that frames the thesis statement: can longitudinal wave propagation in thick cylindrical waveguides be addressed with good engineering practice and finite computational resources?

2. BACKGROUND

The propagation of waves has been a topic of interest in mathematics and mechanics for over 200 years. The basic propagation of elastic waves in solids was extensively developed during the 19th century. Only in the last part of the 19th century has wave propagation in cylindrical rods begun to be investigated. The rich area of research that has developed in this area is considered in this section. The main focus of this section is the research on the propagation of longitudinal waves in circular cross-sectional cylindrical rods. A number of the contributions mentioned in this section are directly relevant to the problem considered in this thesis.

2.1 One-dimensional Wave Equation

One of the first notable contributions to wave propagation in general was made by d'Alembert in 1747. D'Alembert derived a general solution of the one-dimensional wave equation, which provided significant insight into wave propagation. The solution developed, $u(x,t) = f(x-ct) + g(x+ct)$, has the form of an arbitrarily shaped waveform propagating in the positive and negative directions. Consider, if $(x-ct)$ is constant then $f(x-ct)$ is constant. For $(x-ct)$ to remain constant for increasing time, x must increase. This indicates that the shape of $f(x-ct)$ propagates in the positive x direction with increasing time, Fig. 2.1. Similarly, $g(x+ct)$ propagates in the negative x direction. If both functions have the same shape and are sinusoidal then a standing wave is produced. These functions represent propagating disturbances, and these disturbances

propagate without distortion. This is a fundamental characteristic of the one-dimensional wave equation (Graff, 1975).

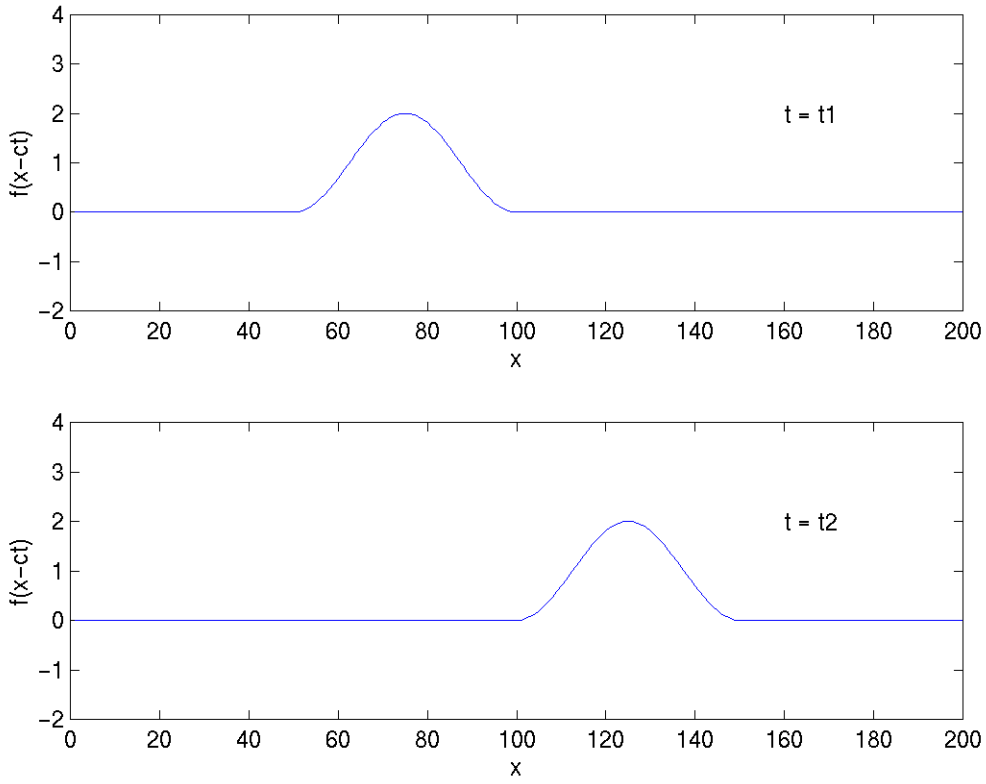

Figure 2.1: One-dimensional wave propagation, $f(x-ct)$, $t_2 > t_1$.

There are two one-dimensional wave equations each related to the limit conditions for an elastic waveguide. The equations have nearly the exact same form, but the wavespeeds are different. Both of the equations are derived from the stress wave equation, $\frac{\partial \tau_x}{\partial x} = \rho \frac{\partial^2 u}{\partial t^2}$. Achenbach (1999) refers to these two wave equations as waves in one-dimensional longitudinal strain and waves in one-dimensional longitudinal stress.

The one-dimensional longitudinal strain wave equation is based on a spatially uniform surface pressure applied to an infinite half space. Any plane perpendicular to the face is a plane of symmetry, so there can be no transverse displacements. Thus the half

space is described by the displacement in the direction of the axis perpendicular to the face, which is a state of one-dimensional deformation. If the axis perpendicular to the face is the x axis, then $\varepsilon_x = \frac{\partial u}{\partial x}$ and $\tau_x = (\lambda + 2\mu)\frac{\partial u}{\partial x}$. The one-dimensional longitudinal strain wave equation becomes $\frac{\partial^2 u}{\partial x^2} = \frac{1}{c_d^2}\frac{\partial^2 u}{\partial t^2}$, where $c_d^2 = \frac{\lambda + 2\mu}{\rho}$. The wavespeed c_d is known as the wavespeed of dilatational waves in an unbounded media (Redwood, 1960).

The one-dimensional stress wave equation is based on a long thin rod in axial tension or compression. If the x axis is along the bar, then the longitudinal normal stress is a function of x and t only and is the only nonvanishing stress. For this case $\tau_x = E\varepsilon_x$; therefore, $\frac{\partial^2 u}{\partial x^2} = \frac{1}{c_0^2}\frac{\partial^2 u}{\partial t^2}$ where $c_0^2 = \frac{E}{\rho}$. The wavespeed c_0 is known as the wavespeed of infinitely long waves in a cylinder, and it is the low frequency limit condition for the first mode of the three-dimensional cylindrical wave equation for longitudinal waves.

2.2 Three-dimensional Wave Equation

For cylindrical geometries, Pochhammer first derived the three-dimensional wave equation in 1876 and Chree separately in 1889. Pochhammer transformed the equations of motion into cylindrical coordinates, and solved the equations for the cases of compressional, flexural and torsional waves in an infinite rod. By applying the boundary conditions for traction free surfaces, the frequency equations were generated. The frequency equation describes the modes of both steady vibration and transient wave propagation (Miklowitz, 1966). The frequency equation is valid for an infinite cylinder with traction free surfaces, and the equation also shows the dispersive nature of the waves for all propagating modes in the three-dimensional cylinder.

Continuing research on longitudinal wave propagation in cylinders was concerned with three areas. Understanding the Pochhammer frequency equation and exploring the equation numerically was the first area. Despite the completeness of the wave equation few analytical results were developed in the beginning because of the complexity of the relationships. Developing approximate solutions for longitudinal wave propagation in semi-infinite bars was the second area. The Pochhammer frequency equation is only valid for an infinite bar. The introduction of additional free boundaries, for example a semi-infinite bar or finite bar, couples equations and adds complexity. The third area was the exploration of a one-dimensional approximation to the Pochhammer frequency equation.

2.3 Continuing Research

2.3.1 One-dimensional Approximations

The exploration of a one-dimensional approximation was the first area to be explored. A. E. Love (1927) developed the first one-dimensional approximation of the Pochhammer frequency equation. Love's equation included the effects of the inertia of the lateral motion, the cross section expanding or contracting. Love formed the equation of motion using the energy method. The equation has the form

$$\rho\left(\frac{\partial^2 u}{\partial t^2} - \nu^2 K^2 \frac{\partial^4 u}{\partial t^2 \partial x^2}\right) = E\frac{\partial^2 u}{\partial x^2} \qquad (2.1)$$

where K is the radius of gyration and ν is Poisson's ratio. Mindlin and Herrmann were the next to develop a one-dimensional approximation. This approximation took into account both the radial inertia and the radial shear of the rod. The approximation has two

modes of wave transmission, and the lower mode shows much better agreement with Pochhammer than does Love (Miklowitz, 1957). Miklowitz (1957) extensively analyzed the Mindlin-Herrmann theory numerically and experimentally. Mindlin and McNiven (1960), revised the one-dimensional approximation to include both the axial shear and the radial modes coupling with the longitudinal mode. These modes also couple with each other in the range of commonly encountered Poisson's ratios.

2.3.2 NUMERICAL RESEARCH

Not long after Love had developed his one-dimensional approximation, work was being performed calculating numerical results from the Pochhammer frequency equation. Field (1931) was one of the first investigators to calculate numerical results. Field compared results from the Pochhammer frequency equation for the first mode to existing experimental data. In the comparison Field concluded that the Pochhammer theory accounted for the right velocity when the frequency approached zero but not when the frequency approached infinity. The Pochhammer frequency equation approaches the wave speed of Rayleigh surface waves, c_R, as the frequency approaches infinity (see Figure 4.1). However, Field expected the wave speed to approach the wave speed in an infinite medium as the frequency approached infinity. Field based his conclusions on low frequency data for solid cylinders, the only data available at the time. That data is roughly analogous to low frequency data for fluid filled cylinders. The high frequency data for fluid filled cylinders shows that the phase velocity approaches the wave speed in an infinite medium, so Field concluded the same must be true for the phase velocity in a solid cylinder.

Bancroft (1941) followed Field's research and explored the effect of Poisson's ratio on the first mode dispersion curve. Bancroft's results were in good agreement when compared to experimental data published by Shear and Locke (1939). Bancroft argued against Field's conclusions. Bancroft stated, "In the case of the infinite medium, the wave involves no motion in the plane of the wave front, and the displacement is uniform. In the case of a long bar, motion in the plane of the wave front is inevitable, and the displacement is far from uniform. It is hard to see how a valid analogy can be drawn between the two cases."

In all of the earlier work, only the first mode was explored. Davies (1948) published a paper that among other things plotted the phase velocity of the first three modes of the Pochhammer frequency equation and the group velocities of the first two modes. The phase velocity is the speed associated with the propagation of a point of constant phase whereas the group velocity corresponds to the velocity of energy propagation. This is the most well known work in this area. Davies' analytical results were in good agreement with Bancroft. Davies introduced a way to measure the axial and radial displacements separately on a circular bar and produced experimental results using a Hopkinson bar. Davies' results were in good agreement with the Pochhammer theory, and he confirmed the phenomenon of dispersion experimentally (Al-Mousawi, 1986).

There have also been experimental results that appear to not agree with the Pochhammer theory. Tu, Brennan, and Sauer (1955) experiments on a cylindrical bar agree with Field's original conclusions that the phase velocity approaches the wavespeed in an infinite medium as $\frac{ka}{2\pi}$ approaches infinity. Transducers were used on the ends of the cylinder to both create and receive the pulse, and pulsed longitudinal waves were

used as the input. This discrepancy with the Pochhammer theory is discussed in Section 4.1.

Three of the last major contributions in this area were only concerned with exploring the Pochhammer frequency equation numerically. Onoe, McNiven, and Mindlin (1962) extensively mapped the relation between the frequency and propagation constant for axially symmetric waves in an infinitely long isotropic cylinder. Real, imaginary and complex propagation constants were calculated for a large frequency spectrum. The influence of Poisson's ratio was also further developed. Zemanek (1972) confirmed theoretical results with experimental results. A most recent contribution has been the work of Peterson (1999) involving the reconstruction of multi-mode waveguide signals, using the Pochhammer-Chree Solution, that are comparable to those measured in experimental configurations.

2.3.3 Semi-infinite and Finite Bars

The approximation for a semi-infinite bar of circular cross-section is also an area of continuing research. It is only within the past 50 years that a three-dimensional equation has been considered to approximate a semi-infinite bar and, ultimately, a finite bar. One of the first approximations was by Skalak (1957) who derived an approximate solution for the impact of two semi-infinite cylinders. The theoretical results agreed with experimental results at long times. Not long after Skalak, Folk et al (1957) developed a solution for a semi-infinite bar loaded with a step pressure function at the end. A pressure was applied to the end of the bar, and the end of the bar was constrained from displacing laterally. The mixed end conditions were used to uncouple the equations of motion. Shook and Curtis (1957) showed experimentally that the mixed end condition

solution predicted accurately the main features of the signal in a semi-infinite bar for distances larger than 20 diameters. Kennedy and Jones (1969) used the method of Folk et al. (1957) to investigate the axially symmetric longitudinal response of a semi-infinite elastic bar to a pressure step end loading. Goldberg and Folk (1993) extended the method of Folk et al. (1957) to allow it to be used for the pure-end-condition problem. Goldberg and Folk obtained the solution to two mixed-end-condition problems, and used these solutions to solve the pure-end-condition problem.

Other recent work has dealt with composites and anisotropic materials. Nayfeh and Nagy (1995) describe axisymmetric waves in anistropic layered cylinders with specific applications to fiber systems used in composites. Laverty (2000) developed a general approach for the characterization of a layered transversely isotropic cylinder.

In addition several papers review the research performed over the years. The review paper by Julius Miklowitz (1966) covers the research up until 1964. Al-Mousawi (1986) reviews mainly the experimental side, and Thurston (1978) reviews elastic waves in rods and clad rods through August 1977. A monograph on elastic waveguides was also published by Redwood (1960)

2.4 Summary

It has only been within the last 50 years that analytical solutions for elastic wave propagation in even the simplest cylindrical geometries have become available. Despite the simplicity of the cylindrical geometry the mechanical relations are very complex. For even a slightly more complex geometry no exact analytical solution exists. It is in these areas that the finite element method (FEM) can be very useful.

3. COMPUTATIONAL RESOURCES

Prior to the recent development of ample computational resources, the numerical solution of elastodynamic problems has typically relied on boundary element formulations to reduce the dimensionality of the problem. However, unlike FEA, boundary element methods (BEM) are difficult to integrate into a general-purpose analysis code, and there are few general-purpose codes commercially available. Conversely, there are many commercially available FE programs that have been extensively developed. As a result, the potential for FEA continues to be explored for this important class of problems. A need persists; however, to understand the computational cost of FEA in elastodynamics and to provide design tools to assist researchers in elastodynamics. In particular, the resolution that is required for a numerical simulation of multiple propagating modes in a solid has created difficulties in prior research (Valle, 2000). For this reason some types of problems require that analytical or semi-analytical solutions be used from a practical perspective. However, only highly simplified geometries can be used for these cases, so finite element solutions are very important.

A primary objective of this research is to provide perspective regarding the role of FEA and analytical solutions in elastodynamic problems. The role of analytical and numerical solutions is somewhat more complex for elastodynamics problems because of the need to time step solutions as well as to discretize the physical domain. The increased dimensionality has reduced the applicability of FEA to elastodynamic problems. Some analytical solutions contrast sharply with FEA in terms of computational costs since they

can usually be run in a math program on a personal computer to produce numerical results. These results are generally obtained with far lower computational demands than numerical results from a finite element analysis. Thus the objective is to further expand the understanding of the spatial and temporal resolution required for FE analyses of elastodynamic problems. On that basis an understanding of potential limitations on FE code and the practicality of FE analyses of elastodynamics can be assessed.

3.1 Finite Element Method

For dynamic modeling there are two finite element methods available. The first and more traditional method is the implicit method. The implicit method is typically used for static analyses and dynamic analyses with quasi-static loading or long time responses. For dynamic analyses the implicit method consists of five steps. First, the displacement equation of motion, $m\ddot{u} + c\dot{u} + ku = F(t)$, is formed for each element. Next, a Newmark *beta* method is used to obtain the system equivalent contribution for each element. All of the element contributions are assembled, $[K_{equiv}]\{\Delta u\} = \{\Delta F_{equiv}(t)\}$. The changes in displacements are determined by inverting the K_{equiv} matrix. The displacements, velocities, stresses, and strains are updated, the time is incremented and the process repeats. The primary computational effort is the matrix inversion (Bennett, 2000).

The explicit finite element method is the second method, and it is used primarily for wave propagation and simulating short time transient responses, i.e. impacts, blasts, etc. (Bennett, 2000). There are four steps in the explicit method. First, all of the force contributions from all the nodes in an element are summed. An acceleration is calculated by dividing the sum of forces by the mass. The velocity and displacement are calculated

from the acceleration, and finally the time is incremented. For example, consider a cantilevered bar with a force on the end in the axial direction. In the first increment the acceleration of the first node is calculated from the applied load. The acceleration is integrated over the increment of time using a central difference rule to determine the velocity. The velocity determines a strain rate and the strain in the element is determined from the integration over the time increment of the strain rate. The stress in the element is calculated from the strain and a force on the next node is determined. The process is explicitly incremented. Thus, for the next time increment, an applied force remains on the first node, but a force is also on the first and second node from the stress in the element. The process continues as the forces propagate along the bar. The required time increments for the explicit method are smaller than the implicit method in order to maintain stability. However, the calculations at each step are simple, so the computer can proceed through the time steps more quickly (Getting Started with ABAQUS/Explicit, 1998).

For either FE method, in order to resolve the wave front, the Courant condition must be satisfied. The Courant condition states that the wavefront cannot travel farther than one element in one time step. This ensures the effect of being able to resolve the wavefront, and any disturbance that is propagated will retain its shape unless there are multiple frequencies that excite higher modes or the frequencies are high enough to feel the effects of dispersion. Therefore, the implicit and explicit finite element methods both require a small time step, but the explicit time step is still smaller than the implicit time step.

The explicit method was used for the models in this thesis for two reasons. In order to resolve the wave front, the time step has to be small for both the implicit and explicit methods. However, the explicit method requires considerably less computational

time per time step. The explicit method is also linearly scalable. If the number of elements doubles the computation time doubles. The computation time quadruples with twice as many elements for the implicit method because of the matrix inversion[1].

The FE program used for this research was ABAQUS (version 5.8.1.4) by Hibbitt, Karlsson, and Sorenson, Inc. ABAQUS can solve dynamic problems with either an implicit method or an explicit method. An axisymmetric element was used for the model because in finite element analyses circular cross-sections lend themselves to the axisymmetric element. Also, this thesis is concerned with longitudinal wave propagation, which has no theta dependence in cylinders with circular cross-section.

3.2 Computer System

The objective of this thesis is to provide insight into the computational cost of modeling wave propagation. Computers continue to develop rapidly in their capabilities; thus, the computer system used for this research must be put into perspective to understand the computational cost and limits of the FE model.

The type of chip and computer can make a large difference in the computational abilities. Different chip architectures can affect efficiency; so more than clock speed is required to assess the computational speed of the machine.

The research for this thesis was performed on two computers, both SGI Power Challenge L 8xR10000. The first machine, named Colorado, had eight 195 MHz processors and 2048 megabytes of RAM. Half of the processors had one megabyte of level 2 cache[2] and the other half had two megabytes of level 2 cache. The second machine, named Columbia, had eight 195 MHz processors and 4096 megabytes of RAM. All of

[1] This true in general; however the times vary because of computational tricks.

Columbia's processors had four megabytes of level 2 cache. Both systems were about 5 years old and used versions of the operating system IRIX 6.5.

These computers can be compared to others using a benchmark. Standard Performance Evaluation Corporation (SPEC) has established a relevant set of benchmarks for performance evaluation of modern computer systems (www.spec.org, 2000). Currently, one of the benchmark suites that has been tested on a large number of computers is the CFP95. The CFP95 benchmark suite consists of 10 benchmarks ranging from vectorized mesh generation to weather prediction to solving Maxwell's equations. These benchmarks measure out of cache memory and CPU performance. The manufacturer runs each of the benchmarks on their computer, and the runtime is recorded. The run time is compared to a reference time. A ratio is produced from the reference time divided by the runtime. The ratios of all the benchmarks for a certain computer are averaged. This average number is used to compare different computers. The speed of the R10000 processor is compared to some more common configurations using the CFP95 benchmark suite, Table 3.1. The finite element program, ABAQUS, did not have parallel processing capabilities on these machines and used only one processor for a single model. Therefore, all of the performance measurements are for a single processor. Data could not be found for the processors with four megabytes of level 2 cache.

[2] Level 2 cache is the amount of RAM contained in the processor.

Manufacturer	Computer System	CFP95 Baseline	FLOPS
SGI	Power Challenge R10000 195 MHz, 1MB L2	11.8	380 Million
	Power Challenge R10000 195 MHz, 2MB L2	13.1	380 Million
Intel	AL440LX Motherboard 433 MHz Celeron	10.4	N/A
	SE440BX2 Motherboard 550 MHz Pentium III	13.8	N/A
	MS440GX Motherboard 450 MHz Pentium II Xeon	13.5	N/A

Table 3.1: Computer comparison based on CFP95 benchmark suite by SPEC.

From Table 3.1 it is evident that the R10000 processors are equivalent to several Intel processors. However, the Colorado and Columbia both had over 2 gigabytes of RAM. Large ABAQUS models require a large amount of RAM, and in some cases the minimum RAM required may be more than 250 megabytes. If a large model is run on a system that does not have enough RAM, virtual memory will be used that requires data be written to the hard drive. This can significantly impact computational time or result in a system crash.

ABAQUS has also developed benchmarks. These benchmarks are solely based on ABAQUS models. There are benchmarks for both the explicit method and the implicit method. However, information could not be found for the computers used in this research. Therefore, a benchmark is included in the appendix. A model similar to the ones used in this research is used on a range of computers. Based on the computation time of the benchmark model, the time for the larger models can be predicted. However, as mentioned before, if memory constraints exist the computational times will not be linearly scalable.

4. TECHNICAL APPROACH AND RESULTS

The phenomenon of dispersion is an element of all wave propagation problems. For all conditions except special cases and limiting conditions, dispersion of a broadband signal is evident. Dispersion is the phenomenon that waves with different wavelengths will travel at different speeds in the same material. Dispersion is present in elastic and electromagnetic waves as well as in waves in fluids. In elastic waveguides, dispersion arises both from geometrical considerations as well as a result of material properties. In this thesis the material used for the model is linear elastic, so the observed dispersion is purely a result of the geometry of the problem. The key description of a wave with dispersive characteristics is the dispersion curve. Dispersion curves show the relationship between the phase velocity and the wavelength of a specific material and geometry, Figure 4.1. Another illustration of dispersive wave characteristics is the group velocity curve. The group velocity, c_g, represents the velocity of energy propagation, $c_g = d\omega / dk$.

Dispersion curves were used in this work to compare the results from the FEA to the analytical results from the Pochhammer-Chree solution. Since prediction of the dispersion curves is a key analytical result of the relevant elastodynamic solutions, the dispersion curve domain is well suited to comparing the fidelity of FEA results to canonical solutions from the literature.

In order to accurately create dispersion curves from a finite element model, it is necessary to know how the element size and time-step affect the accuracy of the model.

The first part of this section describes the numerical experiments performed to determine the element size and time-step that will give accurate FEA results. The case of a single dispersive mode was considered first. The effect of increasing frequency is an increase in the number of modes that propagate in the waveguide. This case was also considered.

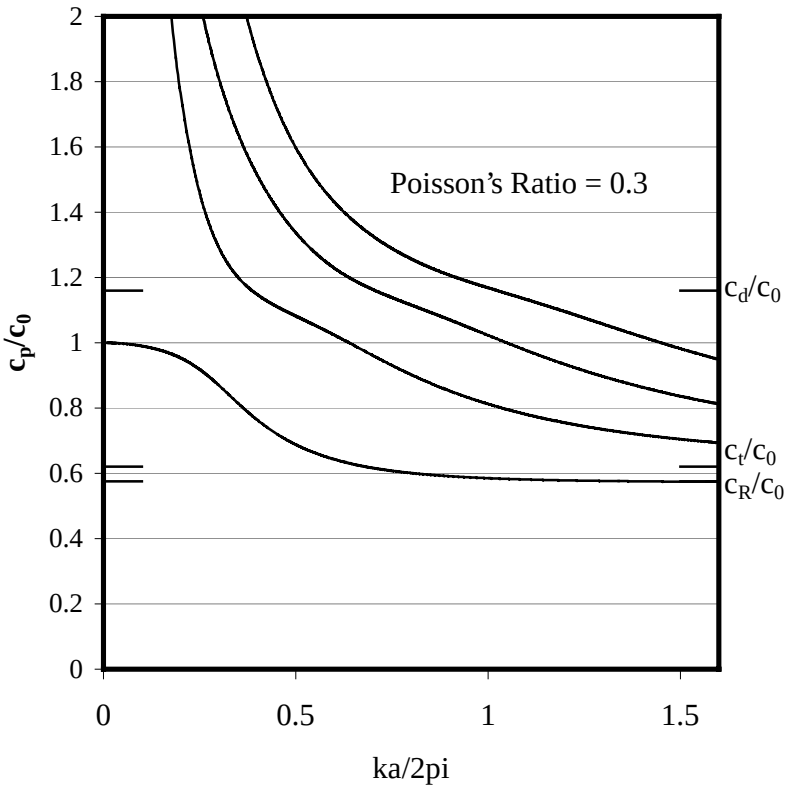

Figure 4.1: Calculated analytical dispersion curves for an isotropic cylinder, $\nu = 0.3$**.**

The second part of this section is concerned with validating the parameters determined in the first section. The parameters were verified by producing three sets of dispersion curves. Running many finite element models, each with a different excitation frequency, created two sets of dispersion curves. The results of each model were plotted to create the dispersion curves. The third set of dispersion curves was created from a single model with a broadband input. The two sets of dispersion curves were compared to

dispersion curves created from the Pochhammer-Chree solution, and the FEA results were validated.

4.1 Numerical Cases

The model used for testing and final analytical validation of the dispersion curves was an axisymmetric model. The model was a simple cylindrical bar with a radius of 0.25 inches (6.35 mm). The length was varied for the cases considered. The bar was modeled as a steel bar with the material properties:

- Young's Modulus, $E = 30x10^6$ psi (26.8 Gpa),
- Poisson's ratio, $\nu = 0.3$,
- Density, $\rho = 7.32x10^{-4}\ lb \cdot \sec^2/in^4$ (7822.8 kg/m^3).

The centerline of the axisymmetric model was fixed in the radial direction. A pressure that was constant across the radius, defined by a user's function, was applied to the circular face of the bar. This was the basic model, and the only changes between models were element size, time step, input pressure function and the length.

The model was a finite length bar in all of the cases considered even though the Pochhammer frequency equation is based on an infinitely long bar. The results of the finite element analyses could be compared to the Pochhammer frequency equation because the waves were not allowed to reflect off of the free end in the FE model. Wave propagation in a finite length cylinder behaves the same in an infinite cylinder until the wavefront reaches a discontinuity such as the end of the bar or a step change in diameter.

4.1.1 Single Mode Propagation

For only a single mode to be present in a waveguide a certain condition needs to exist; the excitation frequency must be below the cutoff frequencies of all of the modes

higher than the first mode. This is somewhat redundant because the first mode does not have a cutoff frequency, so the excitation frequency should be below all of the cut-off frequencies. The cut-off frequency is the frequency at which the wave number is equal to zero. The cutoff frequency also corresponds to the lowest frequency at which a particular mode appears. For example, the second mode cutoff frequency for the 0.25-inch cylindrical steel rod modeled is 306 kHz. Below this frequency the second mode has a complex wavenumber and thus decays exponentially with propagation distance. The cut-off frequency is more generally expressed as a non-dimensional quantity. The non-dimension frequency is expressed as $\frac{\omega a}{\pi c_t}$ where a is the radius, and $c_t = \sqrt{\frac{\mu}{\rho}}$, the propagation velocity of the transverse or shear wave in an unbound media. The non-dimensional cut-off frequency for the second mode is 1.22 when calculated for a Poisson's ratio of $\nu = 0.3$. The first mode is present at all frequencies, so no cutoff frequency exists for the first mode. The single mode waveguide thus corresponds to non-dimensional excitation frequencies below 1.22.

The simplest case of single mode wave propagation is the limiting condition for a thin waveguide. The second limit case, a half-space, can also be directly obtained from the solution for a waveguide. Both of the limit conditions, a long thin rod and a half space, are illustrated by the dispersion curves and the group velocity curves. The dispersion curves in Figure 4.1 illustrate the thin rod limit condition. As $\frac{ka}{2\pi}$ approaches zero, the solution for a long thin rod is obtained. At the low frequency limit, the dispersion curves approach a phase velocity that is constant with frequency at a value of $c_0 = \sqrt{\frac{E}{\rho}}$.

Recall, from the one-dimensional solution of longitudinal wave propagation in a thin rod, this is the velocity of propagation of the non-dispersive wave. However, as $\frac{ka}{2\pi}$ approaches infinity the conditions for an approach to the thick bar limiting case are more complex. To understand the limit case for the half space it is necessary to look at the group velocity curves as well as the phase velocity curves. From the group velocity curves (Peterson, 1994) it is clear that the group velocity of the modes asymptotically approaches the velocity of propagation of a longitudinal wave in an unbounded media. However to observe that only the HIGHEST mode is present in the half-space solution it is necessary to observe that the modes also represent an eigenfunction expansion of the end conditions from the applied excitation pressure. For a point load on a traction free surface of the half-space, the expansion spatially of the applied load corresponds to excitation of only the highest mode. Thus, only the mode with a group velocity that corresponds to the velocity of a wave in an unbounded media, $c_d = \sqrt{\frac{\lambda + 2\mu}{\rho}}$, is excited. Experimental results by Tu (1955) also show that as $\frac{ka}{2\pi} \to \infty$, $c_p \to c_d$. Numerically it is particularly difficult to show that the one-dimensional plane strain wave equation is a limit condition of the Pochhammer frequency equation. The thin rod is a far more direct limit condition of the Pochhammer frequency equation.

To show the single mode, thin rod results, an excitation frequency was chosen to make the value of $\frac{ka}{2\pi}$ close to zero. This low frequency excitation allows the results of the FEA to be compared to the one-dimensional analytical solution for a thin rod. For the first single mode models a frequency of 10,000 Hz was used, corresponding to a non-

dimensional frequency of 0.04. The combination of this frequency and the radius of the rod produced a radius to wavelength ratio, $\frac{a}{\Lambda}$, of 0.02, which correlates to a wavespeed within 0.01% of the wave speed in a thin bar, c_0.

The infinitesimally thin bar solution also requires that the bar be sufficiently long for the required long wavelengths to travel the bar without reflecting within the window of interest. The geometry and boundary conditions were also chosen to help duplicate the thin rod limit condition. The first model used a length to radius ratio of 320. This aspect ratio is suitable for application of the one-dimensional stress wave solution [e.g. Achenbach, 1999]. A constant pressure was applied across the radius to the end of the bar. The load shape was a single period of a haversine, defined as $P(t) = \frac{A}{2}(1 - \cos(2\pi ft))$. The haversine is a single excitation frequency, f, that oscillates between zero and a peak amplitude, A.

ABAQUS also has the capability to use infinite elements to simulate a semi-infinite medium. For the first test-models, the infinite elements were used at the end of the regular elements to eliminate the reflection from the free end and help simulate a semi-infinite bar. However, it was found that the interface between the finite and infinite elements also produced a small reflection. A continuous haversine was applied to the model described above. Figure 4.2 shows a plot of stress versus time at a node located at a position 1/8th of the length of the bar. For this model, one-dimensional theory for a long thin rod predicts the reflection should arrive at this position on the bar at 0.3705 msec. It can be seen that after this time the peaks change due to the influence of the reflection. The infinite elements were removed in subsequent models. The revised models

were the same length but used finite elements for the entire model. The model runs were stopped before sufficient time had passed for the wave to reflect from the free end.

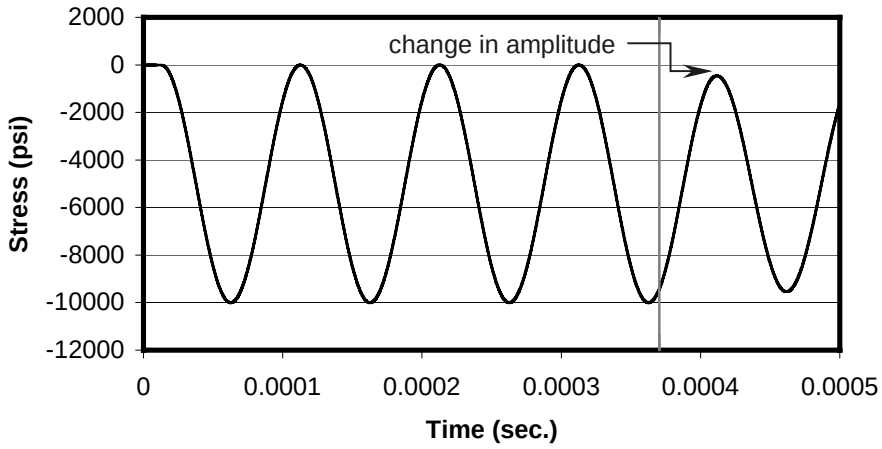

Figure 4.2: The change in amplitude due to a reflection from infinite elements.

Once an adequate model had been determined, the first experiment was run to determine the effect of the element size on the accuracy of the FE model. Models were run with different aspect ratios and element configurations ranging from 10 elements per wavelength up to 160 elements per wavelength. All of the models had the same input of a single haversine and the same time step and length. For each configuration the peak stress was measured for the same point on the bar as well as the amount of the overshoot at the trailing edge of the haversine as shown in Figure 4.3. One-dimensional wave theory explains that a wave should move without distortion. Therefore, the closer the peak stress is to the input amplitude the more accurate the model. Table 4.1 shows the results of the experiment.

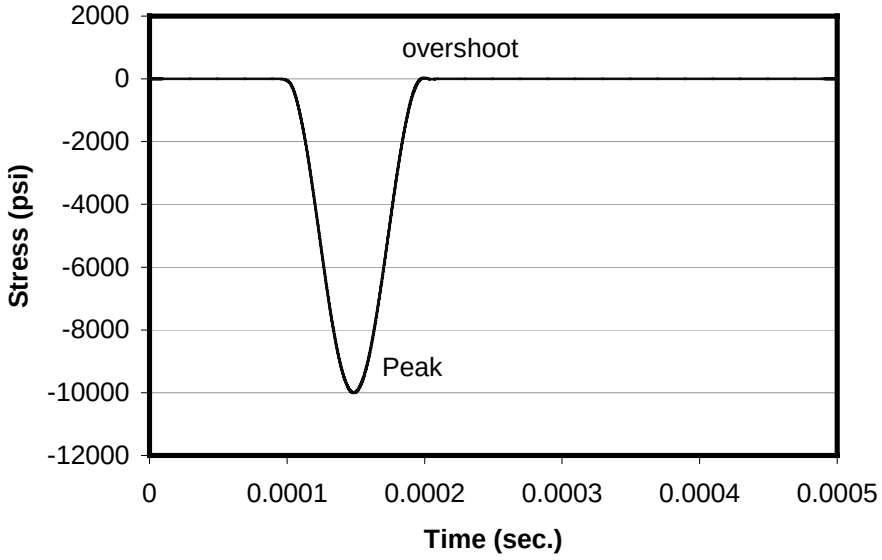

Figure 4.3: Example of results from the first numerical experiment of a single mode waveguide.

Elements per wavelength	Aspect Ratio length:width	Percent Peak Stress Error	Calculated Time step (sec.)
10	1:8	4.651%	7.49E-07
20	1:4	0.860%	7.40E-07
20	1:8	0.864%	3.70E-07
20	1:16	0.864%	1.90E-07
20	1:32	0.860%	9.40E-08
40	1:2	0.161%	7.00E-07
40	1:4	0.111%	3.70E-07
40	1:8	0.102%	1.90E-07
40	1:16	0.102%	9.40E-08
80	1:1	0.036%	6.00E-07
80	1:2	0.039%	3.50E-07
80	1:4	0.024%	1.80E-07
80	1:8	0.020%	9.40E-08
160	2:1	0.002%	4.20E-07
160	1:1	0.002%	3.00E-07
160	1:2	0.001%	1.80E-07
160	1:4	0.000%	9.20E-08

Table 4.1:Effects of element size and aspect ratio on accuracy.

From Table 4.1 it is evident that the number of elements per wavelength has a larger effect on the accuracy of the results than the aspect ratio of the element. The cal-

culated time step in all of the cases shown in the table is the time step calculated by ABAQUS for that specific element size. It is also clear from these results that 40 elements per wavelength is a reasonable starting point for this type of wave propagation model. Good accuracy is obtained with an element size ranging from 40 elements per wavelength to 160 elements per wavelength.

In order to optimize the model it was also necessary to determine an appropriate time step. Using one of the cases from Table 4.1, the time step was varied. The model selected was chosen to have 40 elements per wavelength and the aspect ratio closest to one. In this model the same excitation frequency was used; therefore, only the first mode propagates and without dispersion. The error in the total energy was found to increase with a larger time step, but the error was found to be less than 9.0E-4 in.·lbs. (1.0E-4 N·m) for all cases (results are shown in Table 4.2). This was considered to be a negligible error for the overall model. The total energy is the external work minus the calculated internal energy and kinetic energy, so the value should be zero. The maximum value of the internal energy plus the kinetic energy calculated by ABAQUS was 4.975 in·lbs. (0.5621 N·m) (This value is confirmed analytically in the appendix.) The largest error was found to be less than 0.02% of the maximum internal energy plus kinetic energy. For this particular model the ABAQUS default was approximately 143 time steps per period of the wave. Results for 250 time steps per period showed a good balance between accuracy and model run time. For subsequent calculations 250 time steps per period were used in the calculations.

Timesteps per Period	Timestep (sec.)	Energy Balance (max) (in.*lbs)
1000	3.60E-09	1.00E-05
500	7.20E-09	3.50E-05
333	1.08E-08	8.00E-05
250	1.44E-08	1.30E-05
200	1.80E-08	2.20E-04
100	3.60E-08	9.00E-04

Table 4.2: Comparison of the effects of time step size on calculated energy balance error.

Using the results from the study of the sensitivity of the selection of elements per wavelength and time step, a starting point was obtained for the design of the waveguide models that include multiple propagating modes.

4.1.2 MULTIPLE WAVEGUIDE MODE PROPAGATION

The initial model for the multi-mode waveguides used a haversine excitation with a model that was exactly like the single mode models. In the multi-mode models the excitation frequency used was greater than the cut-off frequency for propagation of the second mode. However, since the haversine used was only a single oscillation of the wave followed by a large number of zeros, significant energy was required at high frequencies to produce the zero amplitude portion of the signal. The existence of the higher frequency components was evident in plots of the stress versus time and stress versus location. What appeared in the results to be noise, was in fact the results of calculations that involve frequencies much higher than the frequency of oscillation of the single oscillation of the haversine. The effects of the higher frequency components obscured the separate modes that should have been evident as the wave propagated down the bar. Based on calculations from the main frequency of the haversine only two modes should propagate. However, because the signal was significantly more broadband, a large number of modes

propagated and the time step and element resolution of the model were insufficient for the actual frequency content of the excitation signal. This broadband signal is also associated with the "overshoot" in the results observed in the single mode case.

A continuous haversine input signal was thus used to ensure the spectrum of the input signal was known. When multiple modes are present the first mode always has the lowest group velocity (velocity of propagation of energy) and has the shortest wavelength at a given frequency. Higher modes travel faster (higher group velocity) and have longer wavelengths at a particular frequency. If a model is expected to have an excitation frequency that is greater than the cut-off frequency of a higher mode, then the model must be configured in a manner that recognizes the presence of shorter wavelengths in the lower modes and higher group velocities in the higher modes. The worst case situation for wavelength and propagation velocity must then be accommodated in selection of element size, model length and model run time. For example, since the first mode has the shortest wavelength, the size of the elements should be based on the first mode. However, the highest mode propagates at the highest group velocity, so the run time of the model should based on the time it takes for the highest mode to reach the end of the model. As a result, higher frequencies result in smaller element sizes to accommodate the shorter wavelengths.

4.1.3 DISPERSION CURVES

For the multi-mode waveguides, points on the dispersion curves were compared to the analytical results to verify the accuracy of the numerical models. Analytical dispersion curves were calculated based on the Pochhammer frequency equation. Newton's

method was used in a Matlab program to calculate dispersion curves for the first four modes (Figure 4.1).

The numerical FE model for the multi-mode waveguide was completed based on the modeling criteria that was determined from the single mode models. Running models with only a single excitation frequency produced a preliminary set of dispersion curves. Each model was excited by a single excitation frequency from a continuous haversine input signal. The excitation frequency excited all of the modes whose cutoff frequencies were below this excitation frequency. Each excited mode produced a point on that mode's respective dispersion curve.

The wave numbers were determined by taking a discrete Fourier transform (DFT) (using a fast Fourier transform, FFT, algorithm where appropriate) of the stress versus location data. The phase velocities, c_p, were determined from the frequency, ω, and the wavenumber, k:

$$k = \omega / c_p \tag{4.1}$$

In order to obtain the dispersion curves that are directly comparable to the analytical results the results were plotted for a range of frequencies.

In order to obtain sufficient accuracy with the discrete Fourier transform used to determine the points on the dispersion curves, a sufficient number of points had to be calculated in the numerical model. An increase in the number of points at a fixed sampling distance on the bar corresponds to an increase in the resolution of the transformed variable. In this case the spatial variable, z, is transformed into the wavenumber, k. The transform pair is:

$$F\{\sigma(z)\} \Rightarrow X[k] = \sum_{z=0}^{N-1} \sigma[z] e^{-j(2\pi/N)zk} \qquad k = 0,1,...,N-1 \tag{4.2}$$

$$F^{-1}\{X(k)\} \Rightarrow x[z] = \frac{1}{N}\sum_{k=0}^{N-1} X[k]e^{j(2\pi/N)zk} \qquad z = 0,1,\ldots,N-1 \qquad (4.3)$$

for the transformation of the stress versus distance into the wavenumber domain. In order to obtain the required resolution however it is important to be cautious regarding the required model size. Although a longer model gives a higher resolution in the wavenumber domain, the increase in computational time does not increase linearly with an increase in length. If a model is doubled in length, the computation time increases by a factor of four. The longer model has twice the number of elements and the number of time steps required for the wave to reach the end of the bar has also doubled.

However, if the disturbance, or elastic wave, has compact support in the time domain, the remaining data in the time record consists entirely of zero values. Therefore, an alternative to making the model longer is to simply pad the data from the numerical model with zero values. Zero padding consists of adding zeros to the end of the data. Zero padding is often used to make the number of data points a power of two, which allows the original Cooley-Tukey FFT algorithm to be used (Cooley-Tukey, 1965). In this application as in other cases where function has compact support, the time domain signal is of finite extent. Zero padding effectively makes the bar longer. The result is new data that interpolates the results from the DFT algorithm. More accurate wavenumbers are then obtained because of the ability to find the peak values in the transformed data. Zero padding will also cause additional low wavenumbers to appear. These additional wavenumbers can obscure the results of small amplitude low wavenumbers corresponding to excited modes. Figure 4.4 illustrates the effects of zero padding on the Fourier transform of the spatial data. In Figure 4.4 the second and third mode wave numbers are shown at a frequency that is just below the cut-off frequency for the fourth mode.

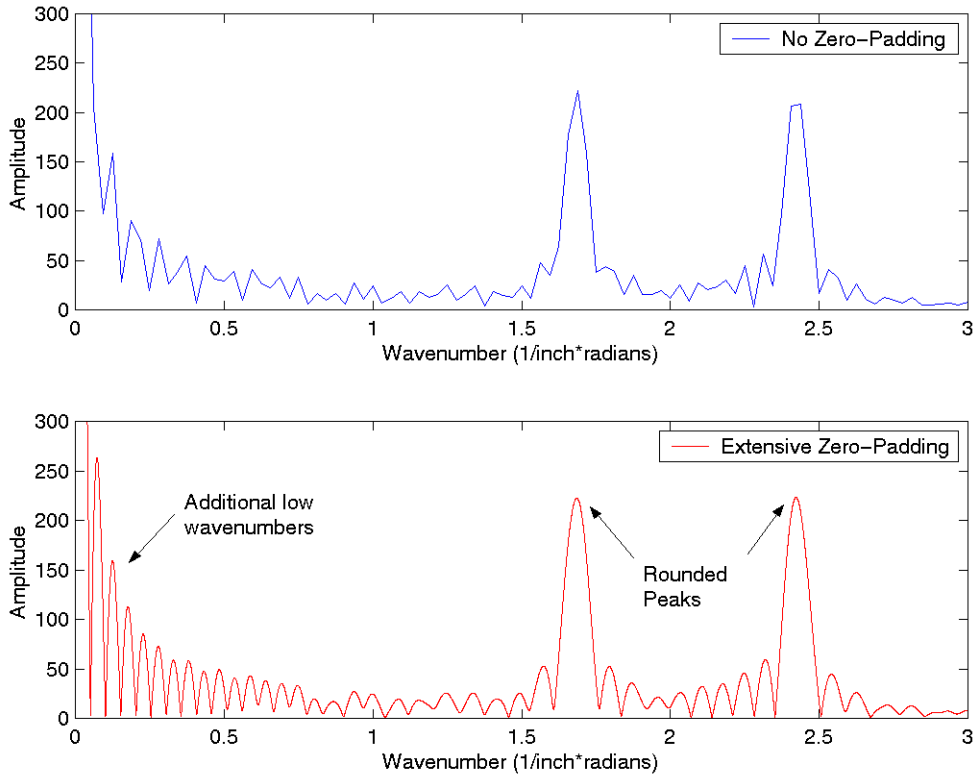

Figure 4.4: Example of the effects of zero padding.

4.1.4 PARAMETER REFINEMENT

It was apparent that the FE model used thus far had not been optimized sufficiently. For the highest excitation frequencies in the desired frequency range the model would take a very long time to run. In order to decrease the time required to run the model at high frequencies while maintaining acceptable accuracy, the parameters had to be explored more finely. Numerical experiments were performed to determine a more accurate minimum acceptable number of elements per wavelength. The experiment to determine the time step was repeated with the new number of elements per wavelength. Finally, a minimum bar length required for acceptable results was also considered.

The first experiment explored the number of elements per wavelengths more closely. A frequency was chosen that would excite the first three modes and a standard model was used. Five element sizes were used that produced a range of elements per wavelength between 11 and 41. Extensive zero padding was used with the FFT to help accurately determine the peaks. Table 4.3 shows the accuracy of each mode compared with the analytical solution.

Elements per wavelength	Percent Error K_1	Percent Error K_2	Percent Error K_3
41	0.3%	0.2%	0.5%
29	0.6%	0.3%	0.4%
23	0.9%	0.4%	0.9%
17	1.7%	0.7%*	3.4%
11	4.0%	2.1%*	6.8%

Table 4.3: Accuracy of elements per wavelength for multiple mode propagation.

From Table 4.3 it is evident that 30 elements per wavelength maintains reasonable accuracy, around 0.5%. Below 20 elements per wavelength the accuracy drops off rapidly. One interesting observation is that the third mode accuracy decreases as fast as the first mode accuracy. The third mode has a significantly longer wavelength and therefore has more elements per wavelength in the same model. Based on considerations of elements per wavelength, the third mode calculations should be very accurate. With even the coarsest mesh the third mode has more than 80 elements per wavelength. However, the wave number calculated for the third mode is small, and the effects of the Fourier transform are a more significant factor. The values calculated for the second mode, in contrast, seem more reasonable. In Table 4.3 asterisks indicate that values were recorded from the initial Fourier transform without zero padding. With zero padding the wavenumbers were obscured, so in these cases the signal without zero padding was used to find the wavenumbers.

Since a revised number of elements per wavelength was chosen, the number of time steps per period was also reinvestigated. The model for this experiment had 30 elements per wavelength. The excitation frequency was such that only the first mode propagated, but the peak frequency was still sufficiently high that the wave exhibited dispersive characteristics. The number of time steps per period was varied between 300 and 75. Again, the error in the total energy was found to increase with a larger time step, but the error was found to be less than 4.0E-4 in.·lbs. (0.4519 Nm) for all cases (results are shown in Table 4.4). This was also considered to be a negligible error for the overall model. The total energy is the external work minus the calculated internal energy and kinetic energy, so the value should be zero. The maximum value of the internal energy plus the kinetic energy calculated by ABAQUS was 3.5 in·lbs. (0.3954 Nm), and this value is confirmed analytically in the appendix. The largest error was found to be less than 0.01% of the maximum internal energy plus kinetic energy. A similarly small effect was found from varying the time step when calculating the wave numbers. For this particular model the ABAQUS default was approximately 95 time steps per period of the wave. Results for 200 time steps per period showed a good balance between accuracy and model run time. For subsequent calculations 200 time steps per period were used in the calculations.

Timesteps per Period	Timestep (sec.)	Energy Balance (max) (in.*lbs)	K_1 Value (1/inch)
300	1.20E-08	3.50E-05	2.0004
250	1.44E-08	4.50E-05	2.0003
200	1.80E-08	5.50E-05	2.0002
150	2.40E-08	9.00E-05	2.0000
100	3.60E-08	2.00E-04	1.9995
75	4.80E-08	3.50E-04	1.9989

Table 4.4: Comparison of the effects of time step size on calculated energy balance error and wavenumber.

The last set of numerical experiments was designed to determine the length of the bar required for obtaining adequate mode separation. To determine a minimum bar length a single model was run for a long bar. The excitation frequency used excited the first three modes. Wavenumbers were calculated from results at different times. Each time effectively corresponded to a bar with a different length, Fig. 4.5. At the first time increment the wave front had traveled almost 20 inches (508mm, 80 radii). The results obtained for this time increment were equivalent to a bar of this length. Zero padding was used to increase the wavenumber resolution. The results were recorded at three additional times corresponding to bar lengths of 160, 240, and 320 radii. The wavenumbers were calculated to determine the accuracy of the solution for each bar length. Table 4.5 shows the numerical results compared to results from the analytical solution.

Length to Radius Ratio	Percent Error K1	Percent Error K2	Percent Error K3
80	0.23%	0.23%	NA
160	0.31%	0.20%	NA
240	0.31%	0.20%	0.84%
320	0.33%	0.20%	0.51%

Table 4.5: Effect of length on mode separation.

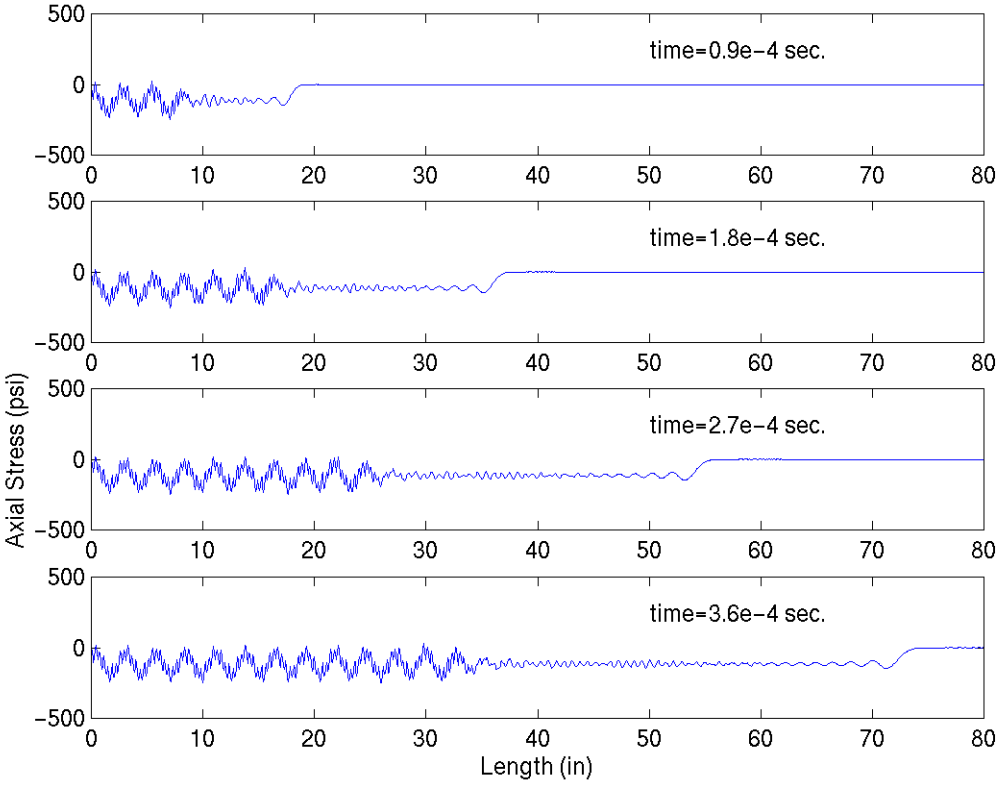

Figure 4.5: Illustration of relationship of time to effective bar length.

Table 4.5 indicates that a smaller length to radius ratio does not affect the accuracy of the wave number, provided that zero padding is used. However, if a wave number is small enough, it may be obscured by the additional peaks at low wavenumbers introduced by the zero padding. This is the case for the third mode at this frequency.

After the series of numerical experiments, three parameters were identified as necessary for modeling multi-mode wave propagation in rods. At least 30 elements per wavelength should be used to provide the required spatial resolution. The element size is determined from the wavelength of the first mode at the highest excitation frequency. The wavelengths associated with higher modes are longer and are thus satisfied automatically. The time step should be at least as small as the time step calculated by ABAQUS if there are at least 30 elements per wavelength; however, a time step equivalent to

$1/200^{th}$ of the smallest period of the excitation frequency is recommended. Finally, the length of the bar should be at least 80 radii long in order to obtain accurate wavenumbers without problems associated with reflection from the free end of the bar.

4.2 Validation

More complete determination of the dispersion curves was based on the modeling parameters from the preliminary study. The dispersion curves were created from a number of FE models of a number of sizes. Three sets of dispersion curves were created. The first set of dispersion curves was created from a large number of models each having a different single excitation frequency. The second set of dispersion curves was created from a single model run many times, each time with a different excitation frequency. The third set of dispersion curves was created from a single model with a broadband excitation signal.

4.2.1 Single Frequency Dispersion Curves

All of the models for the first set of dispersion curves had a length to radius ratio of at least 80, but the element size and time step varied. All of the models had a minimum of 30 elements per wavelength for all of the propagating modes. Therefore at higher frequencies the required element size was much smaller. Table 4.6 indicates the element size and number of elements for several of the models used for these dispersion curves. Figure 4.6 shows the dispersion curves calculated with the FE model compared to the dispersion curves calculated from the Pochhammer frequency equation. The match between the results is very good. Slight variability is evident at low frequencies, and some band limited characteristics are evident.

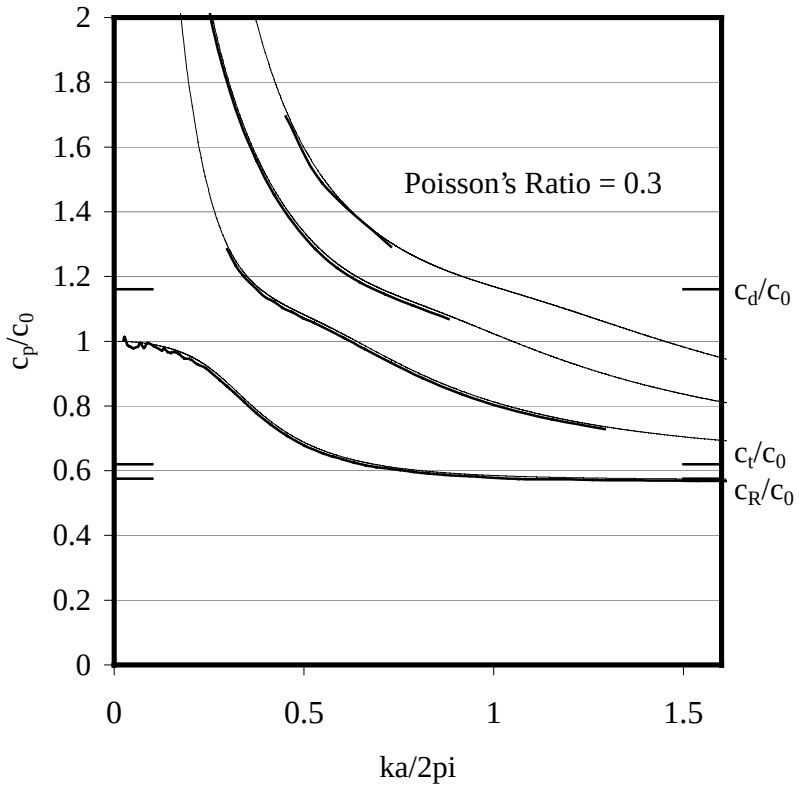

Figure 4.6: Dispersion curves from models with more than 30 elements per wave-length (analytical solution – thin line, FE results – thick line).

Freq. (kHz)	Element Config.
333.3	20x6400
384.6	24x1920
434.8	28x2240
500.0	32x2560
555.6	36x2880
588.2	40x3200
666.7	45x3600
714.3	50x4000
769.2	60x4800

Table 4.6: Element configurations for various frequencies (a = 0.25 inch, 6.35 mm).

To show the effect of reducing the number of elements per wavelength, an alternative set of dispersion curves was created. In the modified approach, the same model was used for all excitation frequencies, although, a single frequency excitation was still used. A model with the same number and size of elements was used for every excitation frequency between just below the 2nd mode cut-off frequency and the 5th mode cut-off frequency. Because the model retained the same configuration for all of the excitation frequencies, the number of elements per wavelength for the first mode ranged between 34 at the lowest frequency and 10 at the highest frequency. The dispersion curves calculated using a consistent model are compared to analytical dispersion curves, Figure 4.7.

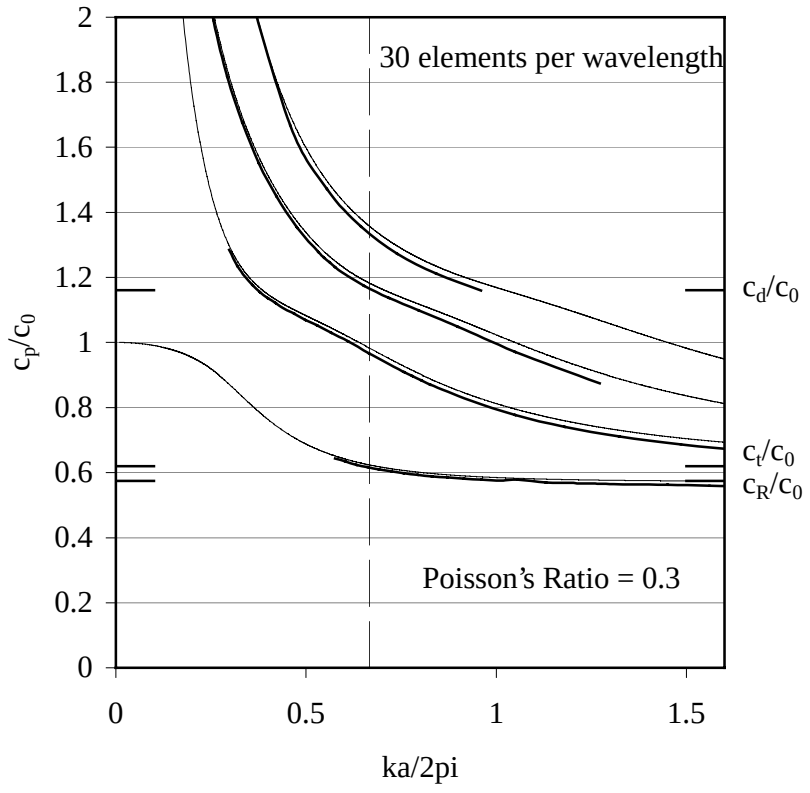

Figure 4.7: Dispersion curves from a single model (analytical solution – thin line, FE results – thick line).

As expected at higher frequencies the accuracy of the FEA decreases due to fewer elements per wavelength. The higher mode dispersion curves appear to diverge from the analytical dispersion curves before there are less than 30 elements per wavelength. The 30 element per wavelength threshold is shown as a vertical line.

4.2.2 BROADBAND DISPERSION CURVES:

To more realistically verify the modeling parameters identified for wave propagation in a cylindrical rod, a broadband model was considered. The broadband model made it possible to produce a set of dispersion curves from a single model. The broadband signal included frequency content from zero up to the fifth mode cut-off frequency. Thus four modes were present in the model.

Use of broadband excitation adds some complexity when determining the points for the dispersion curves. For the models that used a single excitation frequency, a Fourier transform could be applied to the stress versus location data[3] to determine the wave numbers associated with that excitation frequency. If the same procedure was employed with results from the broadband model it would not be possible to determine which wave numbers belonged to particular frequencies. Therefore, an extra step is required.

For the broadband model, stress versus time data was recorded at equally spaced points along the bar. The effective result from this approach is that for each point along the bar a frequency spectrum in time is created by the use of a Fourier transform. The shape of the amplitude of the frequency spectrum for each point along the bar was different; however, the spectrum was calculated for the same frequencies at each point. For each frequency, a wavenumber spectrum in the space domain was then created. The am-

[3] The data was recorded at a time when the first wave was near the end of the bar.

plitude of a certain frequency was taken from each of the frequency spectrums for the points along the bar. These points were used to create the wavenumber spectrum in the space domain using another Fourier transform or another spectral analysis method. From the spectrum in the space domain the wavenumbers were determined for each frequency and dispersion curves were plotted. This process is illustrated in Figure 4.8 with an FFT in the space domain. Simply put, a Fourier transform is performed in time and then in space. The transform pairs appear in eqns. 4.4, 4.5, 4.6, 4.7.

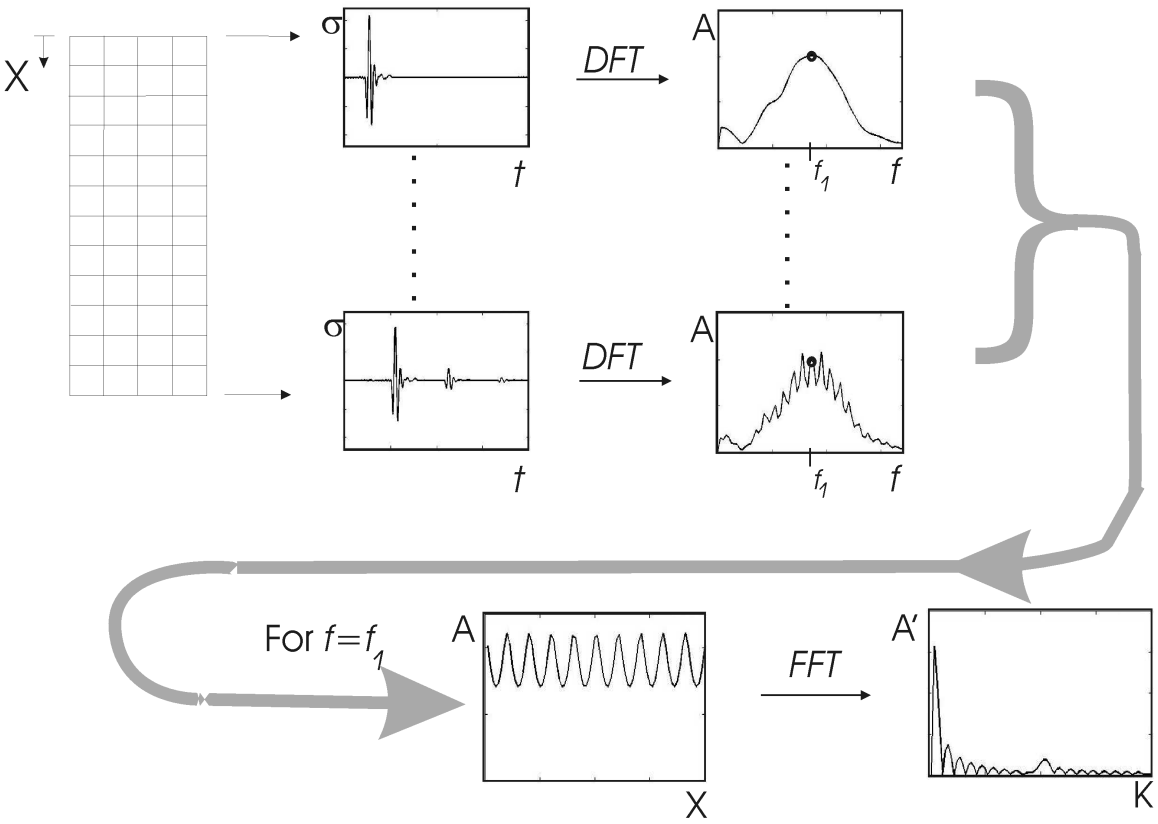

Figure 4.8: Graphical representation of the spectral analysis for broadband results.

$$F\{\sigma(t)\} \Rightarrow A[\omega] = \sum_{t=0}^{N-1} \sigma[t] e^{-j(2\pi/N)t\omega} \qquad \omega = 0,1,\ldots,N-1 \qquad (4.4)$$

$$F^{-1}\{A(\omega)\} \Rightarrow \sigma[t] = \frac{1}{N} \sum_{\omega=0}^{N-1} A[\omega] e^{j(2\pi/N)t\omega} \qquad z = 0,1,\ldots,N-1 \qquad (4.5)$$

$$F\{A_\omega(z)\} \Rightarrow A'[k] = \sum_{z=0}^{M-1} A_\omega[z] e^{-j(2\pi/M)zk} \qquad k = 0,1,...,M-1 \qquad (4.6)$$

$$F^{-1}\{A'(k)\} \Rightarrow A_\omega[z] = \frac{1}{M} \sum_{k=0}^{M-1} A'[k] e^{j(2\pi/N)zk} \qquad z = 0,1,...,M-1 \qquad (4.7)$$

The first broadband input signal used was a Gaussian. The Gaussian is defined as

$$g(t) = e^{-\frac{1}{2}\left(\frac{t-\mu}{\sigma}\right)^2} \sin(2\pi f t) . \qquad (4.8)$$

With the correct parameters for f, t, and μ the highest frequency in the Gaussian will be below the cut-off frequency of the 5th mode. The parameters that determine a frequency range of 0 to 800 kHz are:

- Center frequency, $f = 400kHz$
- Frequency range, $1/\sigma = 800kHz$

These parameters produce the signal in the upper left graph of Figure 4.9. The upper right graph of Figure 4.9 shows the frequency spectrum of the signal. The manipulation of the Gaussian distribution is discussed in the appendix.

After running many models it was found that the Gaussian broadband signal was not providing adequate results. For any particular frequency, wavenumbers could rarely be determined. An alternative broadband signal consisting of the superposition of many frequencies was used instead, eqn 4.9. This broadband signal only contained discrete

$$P(t) = \sum_{n=1}^{N} \frac{A}{2}\left(1 - \cos\left(2\pi n t\left(800{,}000/N\right)\right)\right) \qquad (4.9)$$

frequencies. Better results were generated with this broadband signal. Figure 4.9 illustrates the difference between the signal and frequency spectrum of the Gaussian broadband signal and the superposition of sine waves broadband signal. A narrow band signal is also shown for comparison.

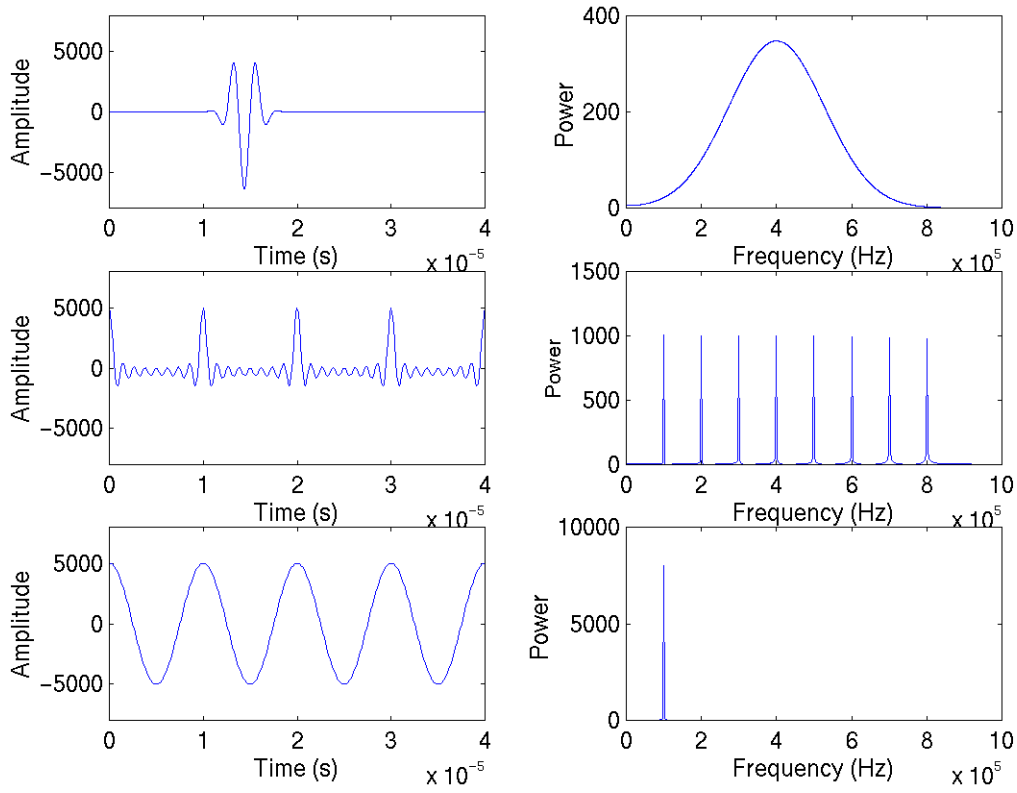

Figure 4.9: Broadband signal and frequency spectrum comparison (top – Gaussian, middle – superposition of sine waves, bottom – narrow band, single frequency).

Although the Gaussian broadband signal did not produce adequate results for dispersion curves it did demonstrate nicely the separation of the modes over time. Figure 4.10 shows the stress versus time and location versus time for a model with a Gaussian input with a frequency range between the second mode cutoff frequency and the fourth mode cutoff frequency (300 – 500 kHz for this case). There is obvious mode separation between the first three modes. This model had a length to radius ratio of 1080. However, the larger length required the element size to be large. At nearly all modes and frequencies less than 30 elements per wavelength were used in the model. Thus, the results showed considerable error. However, the results should be qualitatively correct.

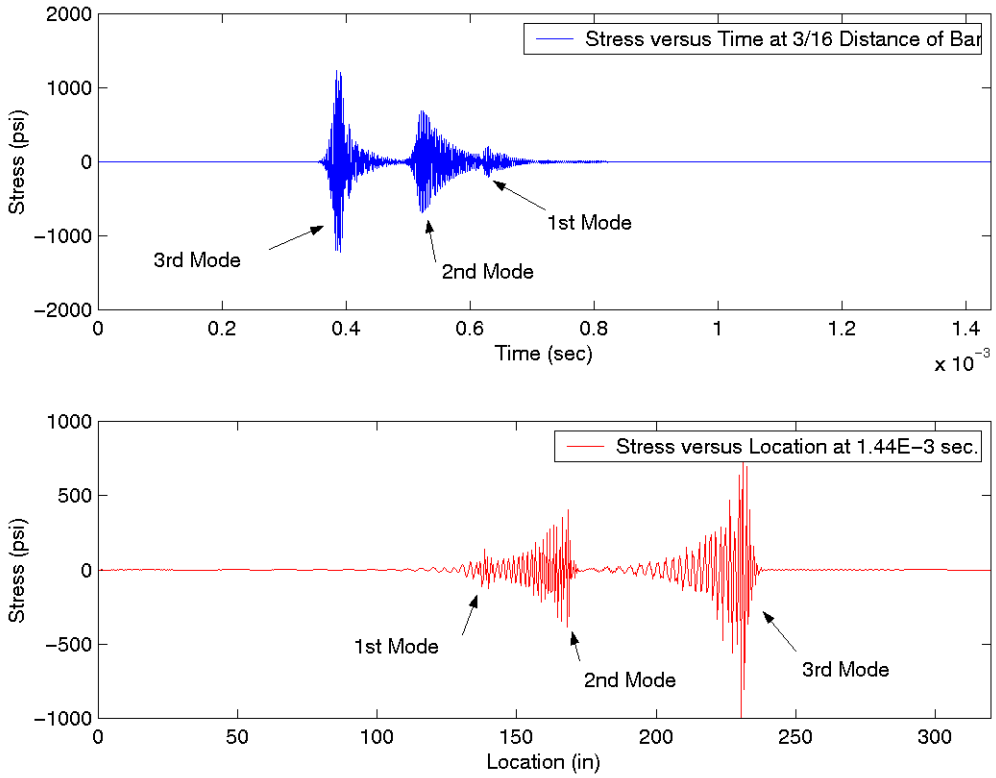

Figure 4.10: Mode separation from Gaussian broadband input signal.

Besides the broadband signal, there were also some issues with the spectral analysis. In the first test models, Prony's method was used to find the wave numbers for each frequency. Prony's method is a way of fitting a function of exponentials to a series of data. However, it was proving difficult to get accurate results[4]. Vollmann, Breu, and Dual (1997) used Prony's method to plot points for dispersion curves from experimental data. Prony's method was chosen rather than a direct implementation of the discrete Fourier transform because of the lack of resolution from the data points with a direct implementation. Prony's method is better able to isolate signals from noise. However, since all

[4] Prony's method was performed on the data from one of the original models that only had a single excitation frequency. It was found that the results from Prony's method were not as accurate as the results from the Fourier transform.

of the data shown is from finite element analysis, noise should be negligible. Zero padding also works well for improving the frequency resolution of the results. Alleyne and Cawley (1990) have shown the use of a two-dimensional discrete Fourier transform to calculate dispersion curves from both experimental and FEA results for Lamb waves. Lamb waves occur in plates and like the waves in the circular cross-sectional cylinder can propagate in multiple modes and show dispersion for higher modes. Alleyne and Cawley concluded that the two-dimensional Fourier transform is applicable to multi-mode propagation with dispersive effects and made use of zero padding to increase frequency resolution. Ultimately a Fourier transform in the time domain and then in the space domain was used to calculate points on the dispersion curves.

In the broadband model additional problems arose exciting all of the modes and finding all of the wave numbers that should exist for each frequency. At the higher frequencies the wave numbers could not be determined for all of the modes since no obvious peaks appeared in the transform. For the single frequency set of dispersion curves, the problem was solved by applying the excitation frequency to only the inside half of the radius, eqn. 4.10 and 4.11. In this case most of the modes were excited and the wavenumbers were determined. For the broadband excitation the first half of the radius was also excited; however the wave numbers associated with the higher modes at the higher frequencies were not always obtained. Applying the excitation frequency to other combinations of elements on the face did not improve results.

$$P(\omega) = \sum_{n=1}^{N} \frac{A}{2}\left(1 - \cos\left(2\pi n t\left(800{,}000/N\right)\right)\right),\ r < a/2 \qquad (4.10)$$

$$P(\omega) = 0,\ r > a/2 \qquad (4.11)$$

By considering the radial stress distribution for the modes of interest, a more reasonable explanation was obtained for the absence of wavenumbers. From a number of references, the change in shape of the modes with increasing frequency may be found (Zemanek, 1972, etc.) The higher order modes have stress that is localized in the center of the bar. The data that was initially used to find the wave numbers was from the axial stress at the surface of the bar. The magnitude of the stress/displacement at the surface is significantly smaller for some modes at some frequencies. Because finite element analysis makes it possible to characterize stresses at elements and displacements at nodes throughout the model this situation may be addressed. Wave numbers were thus determined from results at ¼, ½, and ¾ of the radius and at the surface of the bar. From these multiple locations it was possible to determine wave numbers for all modes at the full range of frequencies.

Extra peaks that did not correspond to a particular wave number were also evident in the transformed domain. These extra peaks were influenced by the input signal. It was found that if the difference in frequency between consecutive frequencies in the input signal was equal to or smaller than the reciprocal of the run time of the model, the extra peaks were reduced or disappeared. Figure 4.11 shows the wave number spectrum calculated at 440 kHz for identical models with different broadband signals. The top model had 80 frequencies equally spaced over 800 kHz corresponding to a 10 kHz frequency step. The bottom model only had 40 frequencies over the same range corresponding to a 20 kHz frequency step. The run time was 0.0001 seconds, so the reciprocal was 10 kHz. However, at higher frequencies both models exhibited extra peaks. The calculated velocities for these extra peaks remained constant as the frequency increased. The extra

peaks appear to be a consequence of model geometry, and a better understanding will require future research.

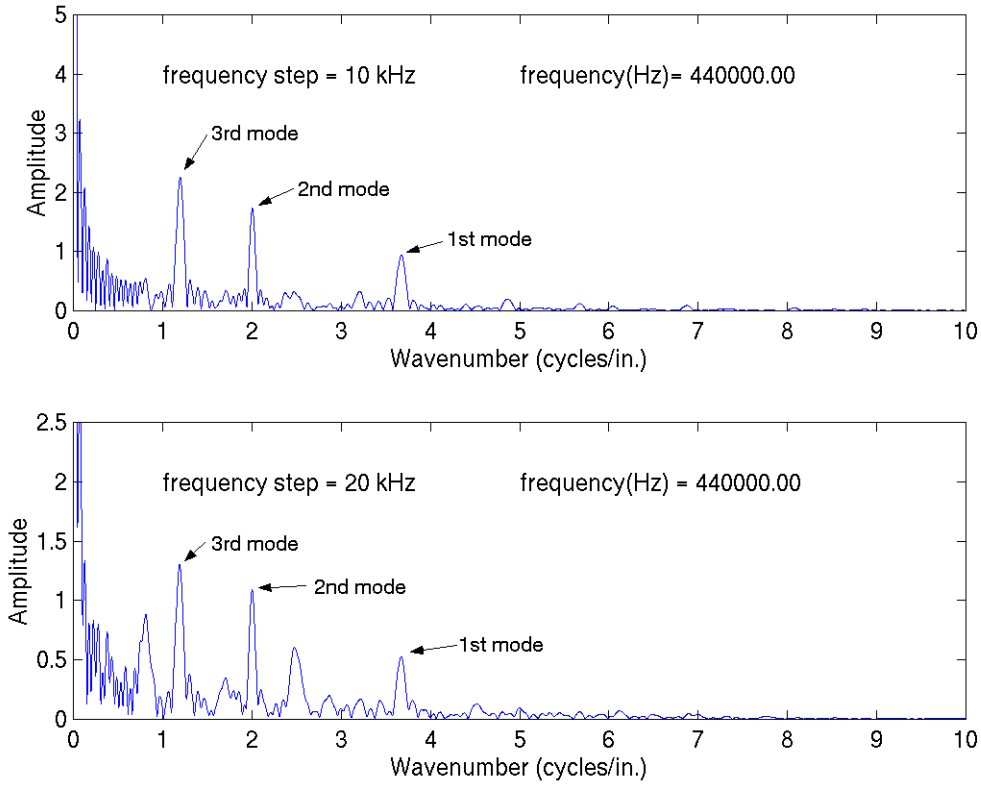

Figure 4.11: Example of wave number spectrum from broadband signal

The final model used the same modeling parameters as the calculations for the first set of dispersion curves. The model used a length to radius ratio of 80. The element size was chosen so the smallest wavelength in the excitation had at least 30 elements per wavelength. A time step of 1/200 of the smallest period was also used. The broadband input signal consisted of 80 frequencies equally spaced between zero and 800,000 Hz superimposed. Using this input the model had 288,000 elements and 20,000 time steps, which took over 18 hours to run on the computer Columbia. The model used over 250 megabytes of RAM, and produced output files requiring over two gigabytes of disk

space. Most of the output files could be deleted upon completion of run. Figure 4.12 shows dispersion curves calculated from the results.

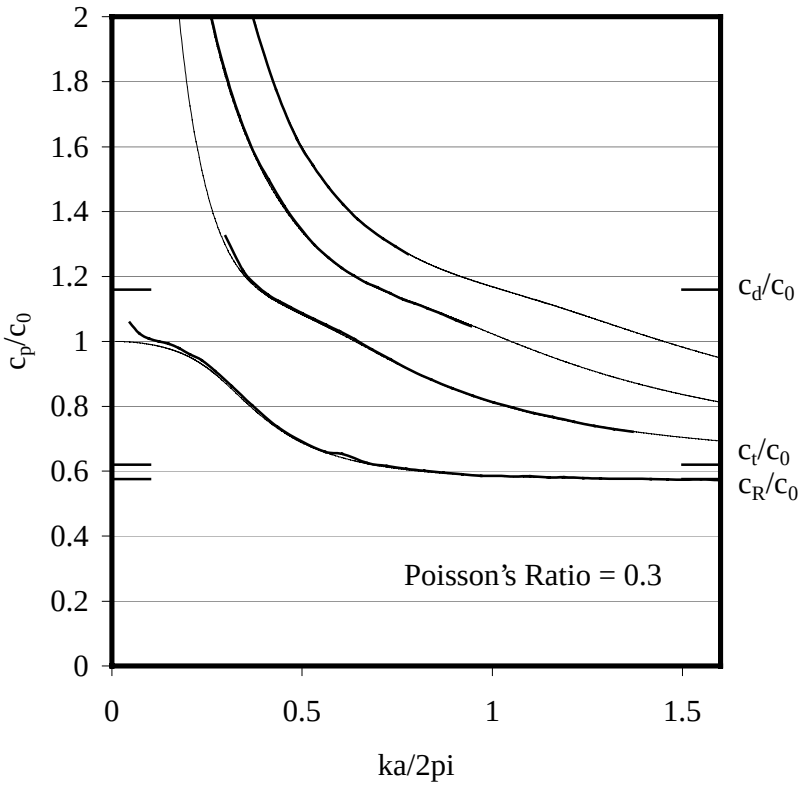

Figure 4.12: Dispersion curves from broadband model (analytical solution – thin line, FE results – thick line).

5. CONCLUSIONS

This thesis is an investigation into the proper application of explicit FEA modeling to the description of elastic waves in solids. The sensitivity to the modeling parameters and the validation of the results were investigated.

5.1 Parameters

The modeling parameters used and which were validated required that 30 elements per wavelength be used for the smallest wavelength and that there be 200 time steps per the smallest excitation period. For the problem considered, less than a 2% accuracy gain would be expected by any further decrease in the time step or element size. However, for the problem considered, the physics of the problem are clearly captured when 30 elements per wavelength are used. If the resolution is decreased the loss of accuracy may result in a loss of physical meaning for the results.

The number of elements per wavelength has the most profound affect on the accuracy of the results. The changes in accuracy are illustrated in the three sets of dispersion curves calculated from the FEA. The dispersion curves calculated from the multiple models can be considered as a baseline for the expected accuracy of the FEA results (Figure 4.5). For the dispersion curves calculated from the single model, only the lowest frequency considered had 30 elements per wavelength. As the frequency increased the number elements per wavelength decreased. The dispersion curves show that the accuracy decreases as the number of elements per wavelength decreases (Figure 4.6). Simi-

larly, for the broadband dispersion curves, the wavelength corresponding to the highest frequency was the only wavelength to have only 30 elements per wavelength. All other wavelengths had more than 30 elements per wavelength (Figure 4.10). The increased accuracy is evident from a comparison between the broadband dispersion curves and the multiple model dispersion curves.

The accuracy of the first mode also seems to affect the accuracy of the higher modes. Based on the dispersion curves created from the single model, the first mode diverged near 30 elements per wavelength, but the other modes diverged well before 30 elements per wavelength. The accuracy of the higher modes diverged near the frequency at which at the accuracy of the first mode diverged. This would imply the accuracy of the first mode affects the accuracy of the higher modes. The interaction of the accuracies of the modes is a key result of this work. This suggests that the physics of the problem are captured by the resolution of the most sensitive portion of the modeling. Once the first mode is no longer resolved, the mode conversion at the bar sides breaks down and the problem becomes physically less descriptive. Hence an absence of a recognition of the effects of multiple modes propagating in a model can result in erroneous results due to improper calculation of wavelengths, and result in errors in using a sufficient number of elements per wavelength.

Issues also arose concerning the time step. Since ABAQUS calculates the time step using the element size, if the element size is small enough then the time step calculated by ABAQUS is sufficiently short as well. The time step is calculated based on the time for a wave with a wave speed of a longitudinal wave in an unbounded medium to travel across an element. The use of a longitudinal wave in an unbounded media for the time step calculations is reasonable, but may lead to an insufficiently short time step. All

of the higher modes travel faster than the longitudinal wave speed at certain frequencies, so a smaller time step may be necessitated. In all of the models presented the time step was calculated by dividing the period of the smallest excitation frequency by at least 200. The time step was consistently smaller than the time step calculated by ABAQUS.

These parameters should be applicable to non-cylindrical geometries. However, the shortest wavelength may not be known even if the highest excitation frequency is known. A conservative value for the shortest wavelength can be calculated using the wave speed of Rayleigh surface waves. From this wavespeed and the highest excitation frequency a value for the wavelength can be calculated.

5.2 Wavenumbers

In order to verify the results, wavenumbers calculations had to be made from the FEA results. Two issues related to the calculation of the wavenumbers used for the dispersion curves were identified. The first issue was the length of the bar/model. The bar had to be long enough to allow the modes to separate. For the single frequency models, a bar 80 radii long was a sufficiently long enough bar. For the broadband model 80 radii was also found to be sufficient. However, both required zero padding (in the FFT in the space domain) to ensure accurate wavenumbers. A longer bar is usually better because of the increased number of data points. The power contained in the noise also increases with length though, so an optimal bar length that does not greatly exceed the signal length is optimal.

The second major issue associated with wavenumbers was exciting all of the modes and finding the complete set of wavenumbers. For the sets of dispersion curves there was trouble exciting all of the modes. It was found that applying the excitation fre-

quency to only the inside half of the radius was sufficient to excite all of the modes. For the broadband model however a problem was encountered in determining the wavenumbers for all of the modes at the higher frequencies. The amplitude of the stress wave varies through the radius of the bar based on the mode shape. The shape of the propagating mode also changes with frequency. Points exist through the radius where the amplitude is zero or quite small. If the radial location selected for calculations is at a low amplitude point the mode may not appear above the noise in a wavenumber spectrum. To ensure that the wavenumber appears in the Fourier transform, data for each mode must be recorded at a point on the radius where the amplitude of the stress is near a maximum. Alternatively, a radial summation of the stress may be possible that effectively mimics the effect of a finite sized sensor such as an ultrasonic transducer.

For each mode a point along the radius was found that produced good wave number results for a large frequency range. For the first mode, data recorded at the surface will produce good wavenumbers for all but a small range around $\frac{a}{\Lambda} = .375$. The second and third modes are well represented by a point at $3/4 \cdot a$. Finally the fourth mode is best determined from a combination of data from $1/4 \cdot a$ and $1/2 \cdot a$. Further work is needed to develop techniques for selecting these points based on propagating mode shapes known from the analytical solution.

The final issue related to the calculation of the wavenumbers was the distinction between the mode wavenumbers and the extra peaks in the wave number spectrum. The extra peaks appeared with use of a broadband signal that contained a superposition of sine waves. It was found that if the frequency step, which is also the lowest frequency,

was less than or equal to the reciprocal of the run time of the model, the extra peaks were smaller or disappeared.

5.3 Broadband Signal

Additional issues emerged regarding the broadband input signals. The selection of broadband excitation signals must be made considering the trade-offs in the results. The Gaussian broadband signal is a simple analytical signal that is closest to a signal that would be encountered out of a laboratory environment. However, the Gaussian was found to produce poor results in this application. It is reasonable that because of the continuous frequency spectrum the model requires a longer bar for adequate mode separation. The other broadband frequency was the superposition of the sinusoids. This signal is most like a chirp signal used in vibration testing but is hard to reproduce at the frequencies considered. The discrete frequencies produce good wavenumber results with minimal analysis.

5.4 Summary

Modeling parameters developed from this thesis were found to be accurate, to within 1%, while minimizing the computational expense. These parameters include:

- 30 elements per smallest wavelength,
- 200 time steps per smallest excitation period,
- minimum bar length of 80 radii

Additionally, the results of this thesis demonstrate that:

- a two-dimensional discrete Fourier transform can be used to obtain dispersion curves from FEA results,
- barriers continue to exist in the modeling of broadband excitation signals,
- careful consideration of mode shape should be made to ensure sufficient data is processed,

- modeling should be based on worst case modes, highest mode for model length, lowest mode for element size.

Continuing research should include determining the effects of element aspect ratio, determining the best spectral analysis methods, determining the best broadband signal, determining the best location in the bar to record data, and finally, determining the best data to record.

6. REFERENCES

ABAQUS/Explicit User's Manual, Vol. I-II, Version 5.8, 1998, Hibbitt, Karlsson & Sorensen, Inc.

Achenbach, J. D. *Wave Propagation in Elastic Solids*, Amsterdam: Elsevier, 1973 or 1999

Alleyne, D. and P. Cawley. "A Two-dimensional Fourier Transform Method for the Measurement of Propagating Multimode Signals." *Journal of the Acoustical Society of America*, Vol. 89, No. 3, March 1991, pp. 1159-1168

Al-Mousawi, M. M. "On Experimental Studies of Longitudinal and Flexural Wave Propagations: An Annotated Bibliography." *Applied Mechanics Reviews*, Vol. 39, No. 6, June 1986, pp. 853-865

Aristégui, C., P. Cawley and M. Lowe. "Guided Waves in Fluid-Filled Pipes Surrounded by Different Fluids: Prediction and Measurement." Review of Progress in Quantitative Nondestructive Evaluation, Vol. 18. NewYork: Plenum Publishers, 1999, pp. 159

Bancroft, Dennison. " The Velocity of Longitudinal Waves in Cylindrical Bars." *Physical Review*, Vol. 59, April 1941, pp. 588-593

Bennett, Joel. 2000. Personal Communication

Bishop, R. E. D. " On Dynamical Problems of Plane Stress and Plane Strain." *Quarterly Journal of Mechanics and Applied Mathematics*, Vol. VI, Pt. 2, 1953, pp. 250-254

Davies, R. M. "A Critical Study of the Hopkinson Pressure Bar." *Transactions of the Royal Society (London)*, Vol. A240, 1948, pp. 375-457

Dual et al. "Experimental Aspects of Quantitative Nondestructive Evaluation Using Guided Waves." *Ultrasonics*, Vol. 34, 1996, pp. 291-295

Cooley, J. W. and J. W. Tukey. "An Algorithm for the Machine Calculation of Complex Fourier Series." Math. Comput. Vol. 19, no. 2, April 1965, pp.297-301

Fiedler, Ch. and W. Wenzel. "Analytical Approximate 3D Solution for the Longitudinally Vibrating Cylinder." *Archive of Applied Mechanics*, Vol. 66, 1996, pp. 447-459

Field, Geo S. “Velocity of Sound in Cylindrical Rods.” *Canadian Journal of Research*, Vol. 5, 1931, pp. 619-624

Folk et al., “Elastic Strain Produced by Sudden Application of Pressure to One End of a Cylindrical Bar. I. Theory.” *Journal of the Acoustical Society of America*, Vol. 30, No. 6, June 1958, pp. 552-558

Fox, George and C. W. Curtis. “Elastic Strain Produced by Sudden Application of Pressure to One End of a Cylindrical Bar. II. Experimental Observations.” *Journal of the Acoustical Society of America*, Vol. 30, No. 6, June 1958, pp. 559-563

Getting Started With ABAQUS/Explicit. 1998, Hibbitt, Karlsson & Sorensen, Inc.

Goldberg, Irwin S., and Robert T. Folk. “Solutions to Time-Dependent Pure-End –Condition Problems of Elasticity: Pressure-Step wave propagation and End-Resonance Effects.” *SIAM Journal of Applied Mathematics*, Vol. 53, No. 5, October 1993, pp 1264-1292

Graff, Karl F. *Wave Motion in Elastic Solids*, New York: Dover Publications, 1975.

Herczynski, Andrzej and Robert T. Folk. “Orthogonality Condition for the Pochhammer-Chree Modes.” *Quarterly Journal of Mechanics and Applied Mathematics*, Vol. 42, Pt. 4, 1989, pp. 523-536

Hill, Lance. 2000. Personal Communication

Kaul, R. K., and J. J. McCoy. “Propagation of Axisymmetric Waves in a Circular Semi-infinite Elastic Rod.” *Journal of the Acoustical Society of America*, Vol. 36, No. 4, April 1964, pp. 653-660

Kennedy, L. W. and O.E Jones. “ Longitudinal Wave Propagation in a Circular Bar Loaded Suddenly by a Radially Distributed End Stress.” *Transactions of the ASME – Journal of Applied Mechanics*, September 1969, pp. 470-478

Kolsky, H. *Stress Waves in Solids*, New York: Dover Publications, 1963.

Love, A. E. H. *A Treatise on the Mathematical Theory of Elasticity*, 4th Ed., New York: Dover Publications, 1944.

Miklowitz, Julius and C. R. Nisewanger. “The Propagation of Compression Waves in a Dispersive Elastic Rod. Part II – Experimental Results and Comparison With Theory.” *Journal of Applied Mechanics*, June 1957, pp. 240-244

Miklowitz, Julius. “ The Propagation of Compression Waves in a Dispersive Elastic Rod. Part I – Results From the Theory.” *Journal of Applied Mechanics*, June 1957, pp. 231-239

Miklowitz, Julius. “Elastic Wave Propagation.” Applied Mechanics Surveys, Washinton DC: Spartan Books, 1966, pp.809-839

Mindlin, R. D., and H. D. McNiven. “Axially Symmetric Waves in Elastic Rods.” *Journal of Applied Mechanics*, March 1960, pp. 145-151

Nayfeh, Adnan H. and Peter B. Nagy. “General Study of Axisymmertic Waves in Layered Anisotropic Fibers and Their Composites.” *Journal of the Acoustical Society of America*, Vol.99, No. 2, February 1996, pp. 931-941

Onoe, Morio, H.D. McNiven, and R. D. Mindlin. “Dispersion of Axially Symmetric Waves in Elastic Rods.” *Journal of Applied Mechanics*, December 1962, pp. 729-734

Peterson, M. L. “A High temperature Ultrasonic Process Monitoring System Utilizing Signal Processing to Separate Multiple Wave Guide Modes.” Ph.D. diss., Northwestern University, 1994.

Peterson, M. L. “Evaluation of Wood Products Based on Elastic Waves.” Nondestructive Characterization of Material VIII, NewYork: Plenum Press, 1998, pp561

Peterson, M. L. “Prediction of Longitudinal Disturbances in a Multimode Cylindrical Waveguide.” *Experimental Mechanics*, Vol. 39, No. 1, March 1999, pp. 36-42

Peterson, Michael. 2000. Personal Communication

Redwood, Martin. Mechanical Waveguides, New York: Pergamon Press, 1960.

Shear, Sidney K., and Alfred B. Focke. “The Dispersion of Supersonic Waves in Cylindrical Rods of Polycrystalline Silver, Nickel, and Magnesium.” *Physical review*, Vol. 57, March 1940, pp. 532-537

Skalak, Richard. “ Longitudinal Impact of a Semi-Infinite Circular elastic Bar.” *Journal of Applied Mechanics*, March 1957, pp. 59-64

Standard Performance Evaluation Corporation, SPEC, “SPECfp95 Results”, *www.spec.org/cgi-bin/osgresults?conf=cfp95*, Internet, Accessed March 2000.

Thurston, R. N. “Elastic Waves in Rods and Clad Rods.” *Journal of the Acoustical Society of America*, Vol. 64, No. 1, July 1978, pp. 1-37

Tu, L Y., J. N. Brennan, and J. A. Sauer. “Dispersion of Ultrasonic Pulse Velocity in Cylindrical Rods.” *Journal of the Acoustical Society of America*, Vol.27, No. 3, May 1955, pp. 550-555

Tuma, Jan J. and Ronald R. Walsh. *Engineering Mathematics Handbook*, 4th Ed., New York: McGraw-Hill, 1998.

Valle, Christine. “Guided Circumferential Waves in Annular Structures.” Ph.D. diss., Georgia Institute of Technology, 2000.

Vollmann, Johannes, Roger Breu and Jürg Dual. “High-Resolution Analysis of the Complex Wave Spectrum in a Cylindrical Shell containing a Visocelastic Medium. Part II. Experimental Results Versus Theory.” *Journal of the Acoustical Society of America*, Vol.102, No.2, August 1997, pp. 909-920

Zemanek, Joseph. “ An Experimental and Theoretical Investigation of Elastic Wave Propagation in a Cylinder.” *Journal of the Acoustical Society of America*, Vol. 51, No. 1 (Part 2), 1972, pp. 265-283

7. APPENDIX

1. COMPUTER BENCHMARK

The model for this benchmark is an axisymmetric rod, 8 elements by 2560 elements. The rod has a 0.25 inch radius and a length of 80 inches, so the elements are square. The timestep is 2.5E-8 seconds, and the run time is 3.6E-4 seconds. Therefore, there are 14,400 timesteps. The material properties used were those of mild steel. The centerline was fixed in the radial direction, and a continuous haversine was applied to one end of the bar with a period of 1.8E-5 seconds.

The following table shows the computational times for both computers. The largest model is also included for comparison. Element Calculations is the number of elements times the number of timesteps.

	Benchmark Model	**Largest Model**	**Large/Benchmark**
Element Calculations	294,912,000	5,760,000,000	19.5
Colorado – 2 Mb cache	1:06:51 (hms)	23:40:57 (hms)	21.26
Columbia – 4 Mb cache	51:16 (hms)	18:11:17 (hms)	21.28

The table indicates that an increase in time is nearly linear with an increase in element calculations. The extra time is most likely due to data storage and manipulation.

1.1 ABAQUS Input File

```
*HEADING
AXIALLY APPLIED HAVERSINE PRESSURE LOAD ON AXISYMMETRIC CYLINDER
*NODE
1,0.,0.
9,.25,0.
23041,0.,80.
23049,.25,80.
*NGEN, NSET=END
1,9
*NGEN, NSET=MID
23041,23049
*NFILL, NSET=ALL
END,MID,2560,9
*NSET,NSET=CENTERL, GENERATE
1,23041,9
*NSET,NSET=DATA, GENERATE
5,23045,9
*NSET,NSET=ROW, GENERATE
5,23045,1440
*ELEMENT, TYPE=CAX4R, ELSET=SOLID
1,1,2,11,10
*ELGEN, ELSET=SOLID
1,8,1,1,2560,9,8
*SOLIDSECTION, ELSET=SOLID, MATERIAL=STEEL
*MATERIAL, NAME=STEEL
*ELASTIC
30.0E6, 0.3
*DENSITY
7.32E-4
*ELSET, ELSET=ROW, GENERATE
4,19204,1280
*ELSET,ELSET=DATA, GENERATE
4,20476,8
```

```
*ELSET, ELSET=FACE, GENERATE
1,4,1
*BOUNDARY
CENTERL,1
*STEP
CONTINUOUS HAVERSINE PRESSURE INPUT
*DYNAMIC, EXPLICIT, DIRECT USER CONTROL
2.5E-8,3.6E-4
*BULK VISCOSITY
0.0
*DLOAD
FACE,P1NU,1.0
*OUTPUT, FIELD, NUMBER INTERVAL=200
*ELEMENT OUTPUT, ELSET=DATA
S
*NODE OUTPUT, NSET=DATA
U
*END STEP
```

1.2 ABAQUS User File

```
****5****10***15***20***25***30***35***40***45***50***55***60***65***70***
*  FORTRAN SUBROUTINE FOR A HAVERSINE LOAD FUNCTION
************************************************************************
    subroutine vdload(nblock, ndim, stepTime, totalTime, amplitude,
     1  curCoords, velocity, dirCos, jltyp, value)
*
    include 'vaba_param.inc'
*
    dimension curCoords(nblock,ndim), velocity(nblock, ndim),
     1  dirCos(nblock,ndim,ndim), value(nblock)
*
        data pi /3.141592653589793/
    data T /1.8E-5/
*

    do 100 km = 1, nblock
            value(km)=10000.0*0.5*(1.0-cos(2.0*PI*stepTime/T))
100 continue
*
    return
    end
```

2. ENERGY VERIFICATION

2.1 Calculation of External Work from a Continuous Haversine

Approximate a semi-infinite bar with a finite bar. Apply a pressure function of a continuous haversine.

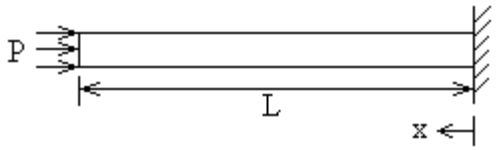

$$P = \sigma = \varepsilon E = E\frac{\partial u}{\partial x} \quad \Rightarrow \quad Pdx = Edu \quad \Rightarrow \quad Px = Eu + C$$

$$\text{at } t = 0 \text{ and } x = 0,\ u = 0 \quad \Rightarrow \quad C = 0$$

$$Work = F \times d \qquad F = PA,\ d = u = \frac{P}{E}x \quad \Rightarrow \quad W = \frac{P^2 A}{E}x$$

$$P = 5000\left[1 - \cos\left(\frac{2\pi}{T}t\right)\right]$$

Since the applied pressure is a function of time, the pressure must be integrated over time.

$$\Rightarrow W_T = \frac{(5000)^2}{30\times10^6}\cdot\frac{(0.25)^2\pi x}{T}\cdot\int_0^T (1-\cos\omega t)^2\,dt = 0.1636\cdot\frac{x}{T}\cdot\int_0^T 1 - 2\cos\omega t + \cos^2(\omega t)\,dt$$

$$= 0.1636\cdot\frac{x}{T}\cdot\left[t - \frac{2}{\omega}\sin\omega t + \frac{\sin(2\omega t)}{4\omega} + \frac{t}{2}\right]_0^T$$

$$= 0.1636x\cdot 1.5$$

$$= 0.2454x$$

Just after one period the front of the wave is at a distance one wavelength from the end of the bar. At this point there is no displacement, so this is equivalent to the fixed end of the bar. Therefore, $L = \Lambda$. For this frequency $\Lambda \cong 0.4981$, $\Rightarrow W_T = 0.1222$. This is the work for one period of the haversine pressure function. The run time of the model was 1.0E-4 seconds, and the period of the haversine was 3.6E-6 seconds. Therefore, there are 27.778 periods of the haversine in the bar at the end of the run time.
$\therefore W_{total} = 27.778\cdot W_T = 3.3944$. ABAQUS calculated approximately 3.5. This is about a three percent difference. The energy calculation by ABAQUS seems correct.
For the single haversine time step experiment, $\Lambda = c_0\cdot T = 202444\cdot 1\times10^{-4} = 20.24$.
$W_T = 0.2454\cdot 20.24 \quad \therefore W_{total} = 1\cdot W_T = 4.967$. ABAQUS calculated 4.975.

3. MATLAB CODE FOR ANALYTICAL DISPERSION CURVES

3.1 Dispersion.m

```
%*********************************************************************
%                   DISPERSION.M
%*********************************************************************
% This Matlab file runs all the m-files needed to produce the
% dispersion curves for a solid isotropic cylinder.
%
% This program only calculates dispersion curves for real wave
% numbers.
%
% The user enters the number of modes desired and the material
% properties.  The cutoff frequencies are calculated and then
% the dispersion curves are calculated.
%
% This file calls the following Matlab files
%   prop.m  - asks for user input
%   cutoff.m - calculates cutoff frequencies for requested
%              number of modes
%   dispcurv.m - calculates and plots dispersion curves
%
% Written by Anthony Puckett March 2000, based on Matlab code
% for a two layered cylinder written by Rich Laverty.
%
%*********************************************************************

prop
cutoff
dispcurv

%*********************************************************************
%  end of script
%*********************************************************************
```

3.2 Prop.m

```
%*********************************************************************
%                   PROP.M
%*********************************************************************
% This Matlab file asks for the material properties, the number
% of modes.
%
% Written by Anthony Puckett, March 2000, based on Matlab code
% for a two layered cylinder written by Rich Laverty.
%
%*********************************************************************
%              MATERIAL PARAMETERS
%*********************************************************************
% a - radius
% E - modulus of elasticity
% rho - density
% nu - Poisson's ratio
% lambda - Lame constant
% mu - lame constant
% cd - dilitational wave speed in unbounded media
% ct - tranverse wave speed in unbounded media
%*********************************************************************

a = input('What is the radius of the cylinder?  ');
E = input('What is the modulus of elasticity of the cylinder?  ');
rho = input('What is the density of the cylinder?  ');
nu = input('What is Poissons ratio?  ');
```

```
lambda = nu*E/((1+nu)*(1-2*nu));
mu = E/(2*(1+nu));
cd = sqrt((lambda+2*mu)/rho);
ct = sqrt(mu/rho);

%*********************************************************************
%             NUMERICAL PARAMETERS
%*********************************************************************
% num - the number of modes to calculate dispersion curves
% success - the number of times in a row that Newton's method
%       must meet tolerance for the iteration to stop
% tol - the tolerance on Newton's method
% maxiter - the maximum iterations of Newton's method
%*********************************************************************

num = input('For how many modes would you like to see dispersion curves?  ');
success=4;
tol=0.001;
maxiter=1000;

save properties

%*********************************************************************
%   end of script
%*********************************************************************
```

3.3 Cutoff.m

```
%*********************************************************************
%                   CUTOFF.M
%*********************************************************************
% This Matlab file computes the cutoff frequencies for the
% requested number of modes (num).
%
% The frequency equations are those derived by Redwood(1960)
% pg. 145 eqns. 6.24 and 6.25.  The former calculates the
% dilitational modes and the latter the transverse modes.
%
% Newton's method is employed to iterate to the final solutions.
% The roots of the bessel functions follow the general approx.
% r(n+1) = r(n) + 3 where r() is a root.  Newton's method will
% iterate for each integer up to 3*num.  There will be several
% duplicates and triplicates, and those are removed.  Finally,
% the dilitational and transverse modes are put together,
% sorted, and the first num modes are selected.
%
% Written by Anthony Puckett, March 2000, based on Matlab code
% for a two layered cylinder written by Rich Laverty.
%
%*********************************************************************
%                   Initialize Variables
%*********************************************************************

load properties

%*********************************************************************
%           Dilitational Modes
%*********************************************************************
% The cutoff frequencies for the dilitational modes are found
% and the duplicates are removed.
%
% freqd - cutoff frequency equation for the dilitational modes
% dfreqd - the derivative of freqd
% subd - a substitution to make the line shorter
% broots - the roots of the dilatational cutoff frequency eqn.
% freqsdil - the cutoff frequencies of the dilitatinal modes
%*********************************************************************
```

```
%*****************************************************************
% Roots found with Newton's method
%*****************************************************************

counter=1;
for x=1:1:3*num
  iter=0;
  goodcount=0;
  while goodcount<success & iter<maxiter
    freqd=x*(besselj(0,x)/besselj(1,x))-2*(ct/cd)^2;
    subd=(-besselj(1,x))*besselj(1,x)-besselj(0,x)*(0.5*(besselj(0,x)-besselj(2,x)));
    dfreqd=(besselj(0,x)/besselj(1,x))+x*(subd/(besselj(1,x)*besselj(1,x)));
    newx=x-freqd/dfreqd;
    if abs(newx-x)<tol
      goodcount=goodcount+1;
    else
      goodcount=0;
    end
    iter=iter+1;
    x=newx;
  end
  broots(counter)=x;
  iters(counter)=iter;
  counter=counter+1;
end
broots=sort(broots);

%*****************************************************************
% Eliminate repeated roots in array broots and write to array
% cutoffd
%*****************************************************************

cutcount=1;
for n=1:1:length(broots)
  if n==1
    cutoffd(1)=broots(1);
    cutcount=2;
  elseif abs(broots(n)-cutoffd(cutcount-1))>tol
    cutoffd(cutcount)=broots(n);
    cutcount=cutcount+1;
  end
end

cutoffd=real(cutoffd);
cutoffd=sort(cutoffd);

%*****************************************************************
% Calculate the cutoff frequencies from the roots.
%*****************************************************************

for n=1:1:length(cutoffd)
  freqsdil(n)=cutoffd(n)*cd/(a*2*pi);
end

%*****************************************************************
%          Transverse Modes
%*****************************************************************
% The cutoff frequencies for the transverse modes are found
% and the duplicates are removed.
%
% freqt - cutoff frequency equations for the transverse modes
% dfreqt - the derivative of freqd
% broots - the roots of the dilitational cutoff frequency eqn.
% freqstran - the cutoff frequencies of the dilitatinal modes
%*****************************************************************

%*****************************************************************
% Roots found with Newton's method
%*****************************************************************

counter=1;
for x=1:1:3*num
```

```
  iter=0;
  goodcount=0;
  while goodcount<success & iter<maxiter
    freqt=besselj(1,x);
    dfreqt=0.5*(besselj(0,x)-besselj(2,x));
    newx=x-freqt/dfreqt;
    if abs(newx-x)<tol & abs(freqt)<1.0
      goodcount=goodcount+1;
    else
      goodcount=0;
    end
    iter=iter+1;
    x=newx;
  end
  broots(counter)=x;
  iters(counter)=iter;
  counter=counter+1;
end
broots=sort(broots);


%*********************************************************************
% Eliminate repeated roots in array broots and write to array
% cutofft
%*********************************************************************

cutcount=1;
for n=1:1:length(broots)
  if broots(n)>0.1 & cutcount==1
    cutofft(1)=broots(n);
    cutcount=2;
  elseif broots(n)<0.1
  elseif abs(broots(n)-cutofft(cutcount-1))>tol & cutcount>1
    cutofft(cutcount)=broots(n);
    cutcount=cutcount+1;
  end
end

cutofft=real(cutofft);
cutofft=sort(cutofft);

%*********************************************************************
% Calculate the cutoff frequencies from the roots.
%*********************************************************************

for n=1:1:length(cutofft)
  freqstran(n)=cutofft(n)*ct/(a*2*pi);
end

%*********************************************************************
% Combine cutoff frequencies, sort, and display
%*********************************************************************

for n=1:1:length(freqsdil)-1
  freqstot(n)=freqsdil(n);
  freqstot(length(freqsdil)-1+n)=freqstran(n);
end

freqstot=sort(freqstot);

for n=1:1:num-1
  fprintf(1,'The cut off frequency for mode %1i is %9.2f %s\n',n+1,freqstot(n),'Hz.');
end

fprintf(1,'Press any key to continue. %s\n',' ');
pause

%*********************************************************************
% end of script
%*********************************************************************
```

3.4 Dispcurve.m

```
%*****************************************************************
%          DISPCURV.M
%*****************************************************************
% This Matlab file computes the dispersion curves for the
% requested number of modes (num).
%
% The curves are calculated from the frequency equation derived
% by Redwood(1960) pg. 137 eqns. 6.19.
%
% Newton's method is employed to iterate to the final solutions
% for each frequency of each curve.
%
% Written by Anthony Puckett, March 2000, based on Matlab code
% for a two layered cylinder written by Rich Laverty.
%
%*****************************************************************
%                  Initialize Variables
%*****************************************************************

load properties
cl=cd;

%*****************************************************************
% Plotting Commands
%*****************************************************************

figure
xlabel('ka /2\pi')
ylabel('c /cp')
axis([0 2.0 0 2.0])
hold on

%*****************************************************************
% Main calculations
%*****************************************************************

for n=1:1:num

%*****************************************************************
% Determine start, step, and end frequency for each mode
% For higher modes the frequency is decreased until cp/co=2,
% that is the start frequency.
%*****************************************************************

  if n==1
    k=0.01*2*pi/a;
    oldk=k;
    wstart=50000*(round(k*sqrt(E/rho)/50000));
    wend=50000*(round((1.5*2*pi/a)*ct/50000));
    wstep=(wend-wstart)/1000;
    pause
  else
    k=(n-1)*0.3*2*pi/a;
    oldk=k;
    wstart=50000*(round(k*1.2*sqrt(E/rho)/50000));
    if wstart<freqstot(n-1)*2*pi
      wstart=50000*(round((freqstot(n-1)*2*pi+50000)/50000));
    end
    w=wstart;
    while w<k*2.0*sqrt(E/rho)
      iter=0;
      goodcount=0;
      while goodcount<success & iter<1000
        p=sqrt((w^2/cl^2)-k^2);
        q=sqrt((w^2/ct^2)-k^2);
        dpdk=-k/sqrt((w^2/cl^2)-k^2);
        dqdk=-k/sqrt((w^2/ct^2)-k^2);
        dq2dk=-2*k;
```

```
        freq1=k^2*q*besselj(0,q*a)/besselj(1,q*a);
        freq2=-0.5*((w/ct)^2)/a;
        freq3=(0.5*(w/ct)^2-k^2)^2*(besselj(0,p*a)/(p*besselj(1,p*a)));
        freq=freq1+freq2+freq3;

        d1freq1=k*2*q*besselj(0,q*a)/besselj(1,q*a);
        d2freq1=k^2*dqdk*besselj(0,q*a)/besselj(1,q*a);
        d3freq1=-k^2*dqdk*a*q;
        d4freq1=k^2*dqdk*a*q*(-besselj(0,q*a))*0.5*(besselj(0,q*a)-
besselj(2,q*a))/(besselj(1,q*a))^2;

        dfreq2=0;

        d1freq3=2*(0.5*(w/ct)^2-k^2)*(-2)*k*(besselj(0,p*a)/(p*besselj(1,p*a)));
        d2freq3=(0.5*(w/ct)^2-k^2)^2*(-dpdk/p^2)*besselj(0,p*a)/besselj(1,p*a);
        d3freq3=(0.5*(w/ct)^2-k^2)^2*(-dpdk*a*p);
        d4freq3=(0.5*(w/ct)^2-k^2)^2*dpdk*a*(-besselj(0,p*a))*0.5*(besselj(0,p*a)-
besselj(2,p*a))/(besselj(1,p*a))^2;

        dfreq1=d1freq1+d2freq1+d3freq1+d4freq1;
        dfreq3=d1freq3+d2freq3+d3freq3+d4freq3;
        dfreq=dfreq1+dfreq2+dfreq3;

        if iter>300
          newk=k-0.6*freq/dfreq;
        else
          newk=k-real(freq/dfreq);
        end

        if abs(newk-k)<0.0001 & abs(freq)<1.0
          goodcount=goodcount+1;
        else
          goodcount=0;
        end

        iter=iter+1;
        k=newk;
      end
      fprintf(1,'w=%8i  k=%6.4f  iter=%3i\n',w,k,iter);
      iters(counter)=iter;
      counter=counter+1;
      kstep=k-oldk;
      if counter==2 & n~=1
        oldk=k;
        k=k*(w+50000)/w
        pause
      else
        oldk=k;
        k=k+kstep;
      end
      w=w-wstep;
    end
    wstart=w+wstep;
    wend=wstart+1000*wstep;
    k=k-kstep;
  end
  clear freqroots;
  clear wavenum;
  counter=1;


%****************************************************************
% Calculate wave number for each frequency using Redwoods
% frequency equation and Newton's method.
%****************************************************************

  for w=wstart:wstep:wend
    iter=0;
    goodcount=0;
    while goodcount<success & iter<1000
      p=sqrt((w^2/cl^2)-k^2);
      q=sqrt((w^2/ct^2)-k^2);
```

```
      dpdk=-k/sqrt((w^2/cl^2)-k^2);
      dqdk=-k/sqrt((w^2/ct^2)-k^2);
      dq2dk=-2*k;

      freq1=k^2*q*besselj(0,q*a)/besselj(1,q*a);
      freq2=-0.5*((w/ct)^2)/a;
      freq3=(0.5*(w/ct)^2-k^2)^2*(besselj(0,p*a)/(p*besselj(1,p*a)));
      freq=freq1+freq2+freq3;

      d1freq1=k*2*q*besselj(0,q*a)/besselj(1,q*a);
      d2freq1=k^2*dqdk*besselj(0,q*a)/besselj(1,q*a);
      d3freq1=-k^2*dqdk*a*q;
      d4freq1=k^2*dqdk*a*(-besselj(0,q*a))*0.5*(besselj(0,q*a)-
besselj(2,q*a))/(besselj(1,q*a))^2;

      dfreq2=0;

      d1freq3=2*(0.5*(w/ct)^2-k^2)*(-2)*k*(besselj(0,p*a)/(p*besselj(1,p*a)));
      d2freq3=(0.5*(w/ct)^2-k^2)^2*(-dpdk/p^2)*besselj(0,p*a)/besselj(1,p*a);
      d3freq3=(0.5*(w/ct)^2-k^2)^2*(-dpdk*a*p);
      d4freq3=(0.5*(w/ct)^2-k^2)^2*dpdk*a*(-besselj(0,p*a))*0.5*(besselj(0,p*a)-
besselj(2,p*a))/(besselj(1,p*a))^2;

      dfreq1=d1freq1+d2freq1+d3freq1+d4freq1;
      dfreq3=d1freq3+d2freq3+d3freq3+d4freq3;
      dfreq=dfreq1+dfreq2+dfreq3;

%*****************************************************************
% If there are more than 300 iterations, the computer may be
% iterating bewteen two numbers; this should fix the problem.
%*****************************************************************

      if iter>300
        newk=k-0.6*freq/dfreq;
      else
        newk=k-real(freq/dfreq);
      end

%*****************************************************************
% Determines when to start the next frequency
%*****************************************************************

      if abs(newk-k)<0.0001 & abs(freq)<1.0
        goodcount=goodcount+1;
      else
        goodcount=0;
      end

      iter=iter+1;
      k=newk;
    end
    fprintf(1,'w=%8i  k=%6.4f  iter=%3i  counter=%5i\n',w,k,iter,counter);
    freqroots(counter)=real(w);
    wavenum(counter)=real(k);
    results(1,counter+(n-1)*1000)=wavenum(counter)*(a/(2*pi));
    results(2,counter+(n-1)*1000)=freqroots(counter)/wavenum(counter)/sqrt(E/rho);
    iters(counter)=iter;
    counter=counter+1;
    kstep=k-oldk;
    oldk=k;
    k=k+kstep;
  end

  fprintf(1,'Press any key to continue. %s\n',' ');
  pause

  plot(wavenum.*(a/(2*pi)), (freqroots./(wavenum))/sqrt(E/rho))


end
```

```
%*****************************************************************
% Write data to file.  cp/co and k*a/2*pi
%*****************************************************************

file = input('What do you want to call this file?  Put single quotations around the
name.');
fid=fopen(file,'w');
fprintf(fid,'%8.4f  %8.4f\n',results);
fclose(fid);

hold off


%*****************************************************************
% end of script
%*****************************************************************
```

4. ABAQUS FILES

4.1 ABAQUS Finite Element Model Input Files

4.1.1 EXAMPLE OF INPUT FILE FOR SINGLE FREQUENCY MODEL

40x3200_hcont17e7.inp

```
*HEADING
AXIALLY APPLIED HAVERSINE PRESSURE LOAD ON AXISYMMETRIC CYLINDER
*NODE
1,0.,0.
41,.25,0.
131201,0.,20.
131241,.25,20.
*NGEN, NSET=END
1,41
*NGEN, NSET=MID
131201,131241
*NFILL, NSET=ALL
END,MID,3200,41
*NSET,NSET=CENTERL, GENERATE
1,131201,41
*NSET,NSET=DATA, GENERATE
30,131230,82
*NSET,NSET=ROW, GENERATE
30,131230,8200
*ELEMENT, TYPE=CAX4R, ELSET=SOLID
1,1,2,43,42
*ELGEN, ELSET=SOLID
1,40,1,1,3200,41,40
*SOLIDSECTION, ELSET=SOLID, MATERIAL=STEEL
*MATERIAL, NAME=STEEL
*ELASTIC
30.0E6, 0.3
*DENSITY
7.32E-4
*ELSET, ELSET=ROW, GENERATE
30,120030,8000
*ELSET,ELSET=DATA, GENERATE
30,127950,80
*ELSET, ELSET=FACE, GENERATE
1,20,1
*BOUNDARY
CENTERL,1
*STEP
TRAPZOIDAL PRESSURE STEP
*DYNAMIC, EXPLICIT, DIRECT USER CONTROL
5.0E-9,1E-4
*BULK VISCOSITY
0.0
*DLOAD
FACE,P1NU,1.0
*OUTPUT, FIELD, NUMBER INTERVAL=200
*ELEMENT OUTPUT, ELSET=DATA
S
*NODE OUTPUT, NSET=DATA
U
**OUTPUT, HISTORY,FREQUENCY=1
```

```
**ENERGY OUTPUT
**ALLWK,ETOTAL,ALLIE,ALLKE
**NODE OUTPUT,NSET=ROW
**U2
**ELEMENT OUTPUT, ELSET=ROW
**S22
*END STEP
```

4.1.2 EXAMPLE OF INPUT FILE FOR BROADBAND FREQUENCY MODEL

60x9600_sum800_80.inp

```
*HEADING
HORIZONTAL BROADBAND PRESSURE LOAD ON AXISYMMETRIC CYLINDER
*NODE
1,0.,0.
61,.25,0.
585601,0.,40.
585661,.25,40.
*NGEN, NSET=END
1,61
*NGEN, NSET=MID
585601,585661
*NFILL, NSET=ALL
END,MID,9600,61
*NSET,NSET=CENTERL, GENERATE
1,585601,61
*NSET,NSET=DATA, GENERATE
61,585661,976
*NSET,NSET=COLUMN, GENERATE
61,585661,36600
*NSET,NSET=ROW, GENERATE
73201,73261,1
*NSET,NSET=TOTAL
DATA, ROW
*ELEMENT, TYPE=CAX4R, ELSET=SOLID
1,1,2,63,62
*ELGEN, ELSET=SOLID
1,60,1,1,9600,61,60
*SOLIDSECTION, ELSET=SOLID, MATERIAL=STEEL
*MATERIAL, NAME=STEEL
*ELASTIC
30.0E6, 0.3
*DENSITY
7.32E-4
*ELSET, ELSET=COLUMN, GENERATE
60,540060,36000
*ELSET,ELSET=DATA, GENERATE
60,575100,960
*ELSET, ELSET=FACE, GENERATE
1,20,1
*ELSET,ELSET=ROW, GENERATE
72001,72060,1
*ELSET,ELSET=TOTAL
DATA,ROW
*BOUNDARY
CENTERL,1
*STEP
GAUSSIAN PRESSURE PULSE
*DYNAMIC, EXPLICIT, DIRECT USER CONTROL
5.0E-9,2E-4
*RESTART,WRITE,NUM=20,OVERLAY
*BULK VISCOSITY
0.0
*DLOAD
```

```
FACE,P1NU,1.0
**OUTPUT, FIELD, NUMBER INTERVAL=200
**ELEMENT OUTPUT, ELSET=TOTAL
**S
**NODE OUTPUT, NSET=TOTAL
**U
*OUTPUT, HISTORY,FREQUENCY=100
*ENERGY OUTPUT
ALLWK,ETOTAL,ALLIE,ALLKE
*NODE OUTPUT,NSET=COLUMN
U2
*ELEMENT OUTPUT, ELSET=COLUMN
S22
*FILE OUTPUT, NUMBER INTERVAL=400
*EL FILE, ELSET=DATA
S
*END STEP
```

4.2 ABAQUS User Files

4.2.1 EXAMPLE OF USER FILE FOR SINGLE FREQUENCY MODEL

havercont29e7.f

```
****5****10***15***20***25***30***35***40***45***50***55***60***65***70***75
*  FORTRAN SUBROUTINE FOR A HAVERSINE LOAD FUNCTION
*************************************************************************
    subroutine vdload(nblock, ndim, stepTime, totalTime, amplitude,
     1  curCoords, velocity, dirCos, jltyp, value)

    include 'vaba_param.inc'

    dimension curCoords(nblock,ndim), velocity(nblock, ndim),
     1  dirCos(nblock,ndim,ndim), value(nblock)

        data pi /3.141592653589793/
    data T /2.9E-6/

    do 100 km = 1, nblock
           value(km)=10000.0*0.5*(1.0-cos(2.0*PI*stepTime/T))
100 continue

    return
    end
```

4.2.2 EXAMPLE OF USER FILE FOR BROADBAND FREQUENCY MODEL

gauss700pulse.f

```
****5****10***15***20***25***30***35***40***45***50***55***60***65***70***75
*  FORTRAN SUBROUTINE FOR A HAVERSINE LOAD FUNCTION                     *
*************************************************************************
    subroutine vdload(nblock, ndim, stepTime, totalTime, amplitude,
     1  curCoords, velocity, dirCos, jltyp, value)

    include 'vaba_param.inc'

    dimension curCoords(nblock,ndim), velocity(nblock, ndim),
     1  dirCos(nblock,ndim,ndim), value(nblock)
```

```
    integer n,km
    real total,f(80)
        data pi /3.141592653589793/

    do 150 km = 1, nblock
       total = 0
       do 100 n = 1, 80
          f(n) = 100*0.5*(1.0-cos(2.0*PI*stepTime*10000.0*n))
          total = total + f(n)
100    continue
       value(km)=total
150    continue

    return
    end
```

5. GAUSSIAN MANIPULATION

This section describes the Gaussian broadband signal and how to choose the correct parameters to produce a specific signal. The advantage of the Gaussian broadband signal is the fact that any range of frequencies can be produced from a single short signal.

The Gaussian broadband signal is made up of two parts. First there is a Gauss distribution, which is defined by

$$P(x) = \frac{1}{\sigma\sqrt{2\pi}} e^{-\frac{1}{2}\left(\frac{x-\mu}{\sigma}\right)^2}$$

The second part of the Gaussian broadband signal is a sine function. Thus, the Gaussian broadband signal has the form

$$P(x) = \frac{A}{\sigma\sqrt{2\pi}} e^{-\frac{1}{2}\left(\frac{x-\mu}{\sigma}\right)^2} \sin(2\pi \cdot x \cdot freq)$$

A Fourier transform of this signal produces another gauss distribution. In other words the frequency spectrum of the gaussian broadband has the shape of a gauss distribution.

There are four variables that can change the signal shape and the frequency spectrum of a Gaussian broadband signal. (These descriptions assume the independent variable is time.)

σ – standard deviation. The length of the gaussian distribution will be just over 6 sigmas. The frequency range around the mean frequency is equal to $1/\sigma$.

$freq$ – mean frequency in Hz, center frequency on the frequency spectrum.

μ – mean, point in time where Gauss distribution is a maximum.

A – a constant to adjust the amplitude of the signal.

The next section shows an example and illustrates how the Gaussian broadband signal and the frequency spectrum are affected by changing each variable.

Example: Create a signal with a frequency range of 0 – 800 kHz.

Solution: The frequency range is 800,000 Hz, so $\sigma = 1/800{,}000 = 1.25E-6$ sec. The mean frequency needs to be 400 kHz, so $freq = 400{,}000$ Hz. The vast majority of the signal should appear at $time > 0$, so $\mu \geq 3 \cdot \sigma$. The mean in this case was chosen to correspond with a trough in the sine wave, $\mu = 5.75 \cdot 1/400{,}000 = 1.4375E-5$ sec. Finally, *A* was chosen to be 0.04 so the peak amplitude was 6000. Figure 1 is a plot of the Gaussian broadband signal and the frequency spectrum.

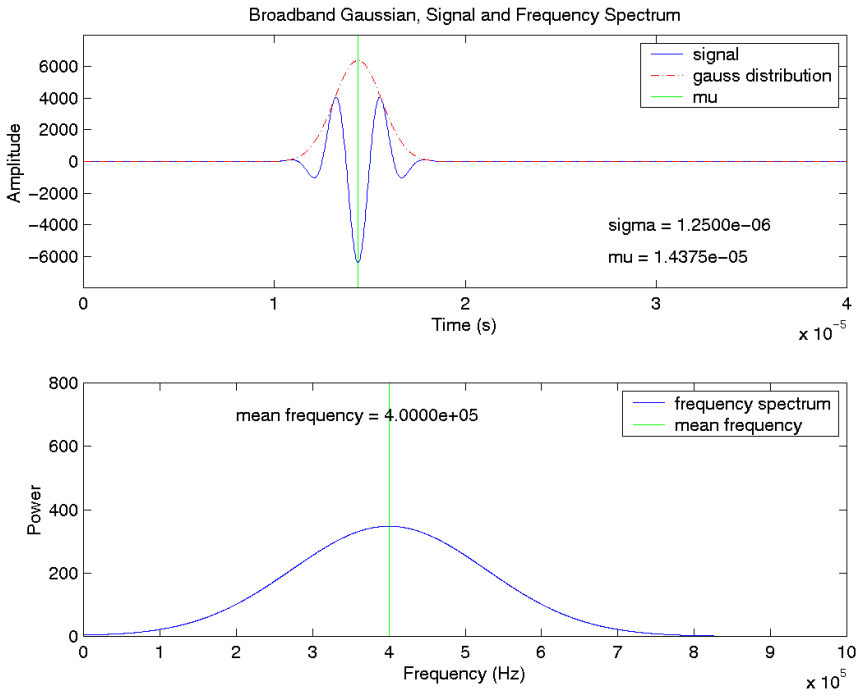

Figure 1: Initial variables

If μ is changed to $\mu = 2.0E-5$ sec. the signal moves in time and the shape is different. The frequency spectrum has the same range but a smaller amplitude, Figure 2.

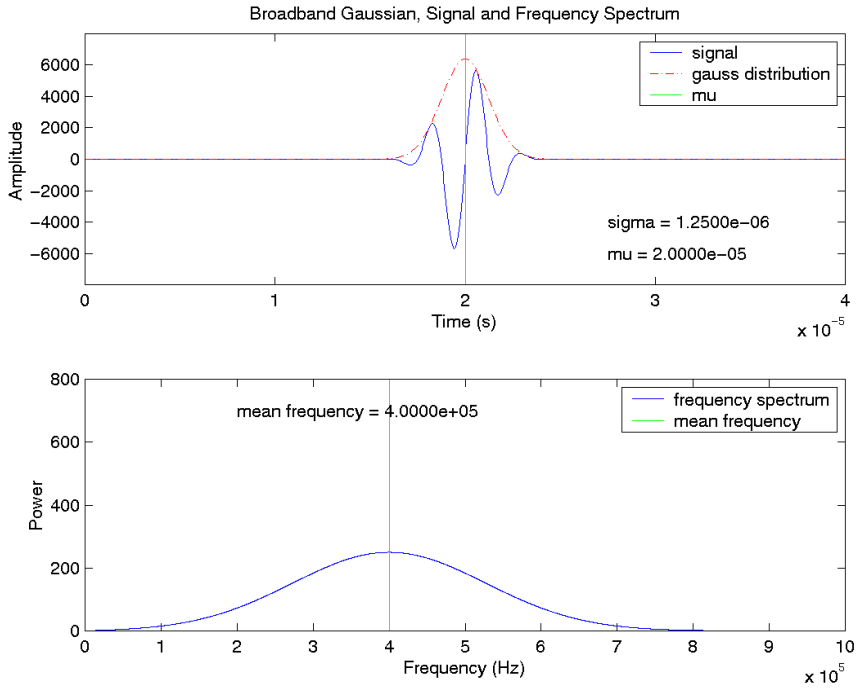

Figure 2: Variable μ increased

Next, the mean frequency is increased, so $freq = 600{,}000$ Hz. The frequency spectrum shifts to the right, and the increase in peaks in the signal also illustrate the higher frequency, Figure 3.

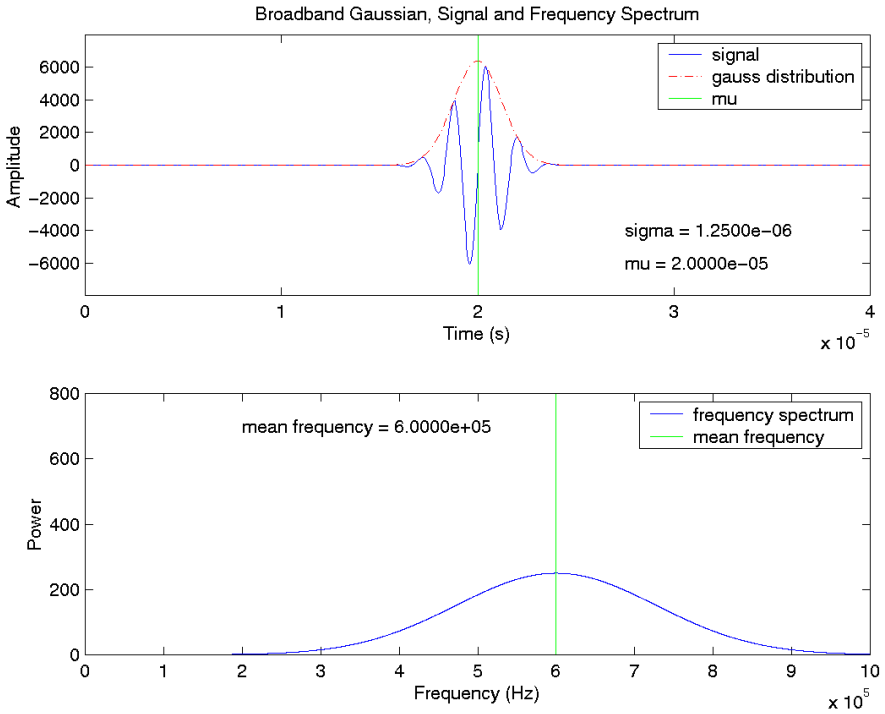

Figure 3: Mean Frequency Increased.

Finally, the frequency range is reduced to 200 kHz by making $\sigma = 5.0E-6$ sec. Since σ increased by four so has the length of the signal. The amplitude of the signal is also smaller.

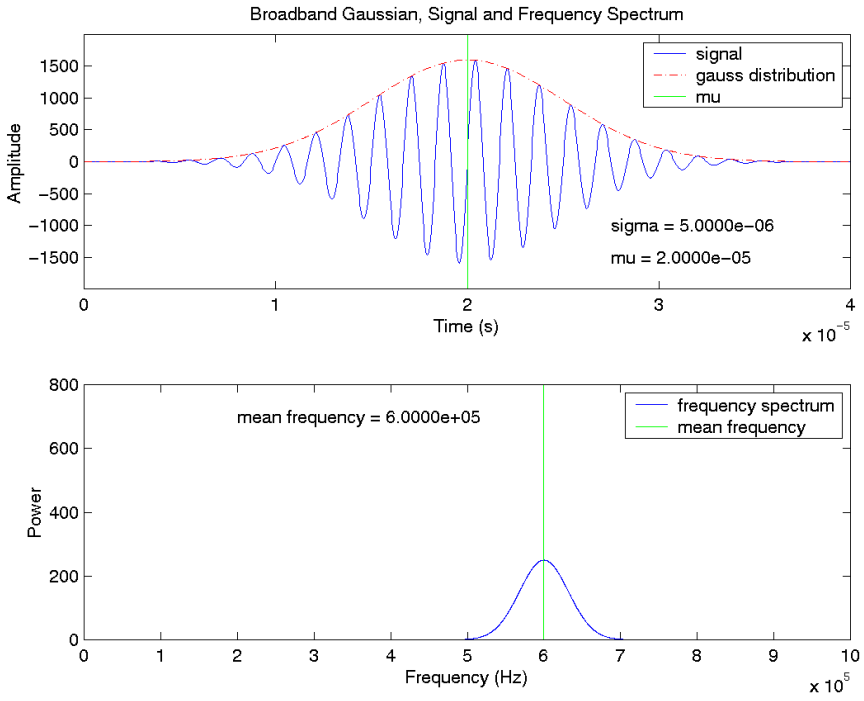

Figure 4: Variable σ increased

6. STEPS FOR EXTRACTION OF DATA FROM ABAQUS RESULTS

6.1 Single Frequency Dispersion Curves

1. Specified column of nodes and elements along axis of bar, usually at ¾ the radius, in ABAQUS input file. Specified type of stress and displacement data for specified nodes, see example code.

```
*NSET,NSET=DATA, GENERATE
30,131230,82
*ELSET,ELSET=DATA, GENERATE
30,127950,80
.
.
*OUTPUT, FIELD, NUMBER INTERVAL=200
*ELEMENT OUTPUT, ELSET=DATA
S
*NODE OUTPUT, NSET=DATA
U
```

2. Ran ABAQUS model.
3. Opened *.odb file in ABAQUS Viewer
4. Selected contour plot of S22 stresses (axial)
5. Under *Tools:Path:Create* created path from previously specified nodes.
6. Under *Tools:XYData:Create* created XY plot of data along path.
7. Plotted stresses at largest time, typically.
8. Under *Report:XY* created XY data file from plot in current view port.
9. Removed titles from data file, so only data was present
10. Ran Matlab file to manipulate data and plot wave numbers.

```
%*****************************************************************
%          M40X3200_HCONT17E7RIGHT.M
%*****************************************************************
% This program reads a text file of element and stress data.
% An FFT is performed on the data in the space domain.
% Wavenumbers for each mode are determined.
%*****************************************************************
% Read data from file
%*****************************************************************

[time, x] = textread('40x3200_hcont17e7right.rpt','%f %f');

%*****************************************************************
% Sample Rate, # of samples divided by the length of the bar.
%*****************************************************************

Fs=80;

%*****************************************************************
% Extensive zero-padding, number of samples a power of 2
%*****************************************************************

tnpts=2.^(ceil(log(length(x))/log(2)))*128;
FFT=fft(x,tnpts);

%*****************************************************************
% Manipulate results of FFT
%*****************************************************************
```

```
NumUniquePts = ceil((tnpts+1)/2);
FFTX=FFT(1:NumUniquePts);
FFTX=abs(FFTX);
FFTX=FFTX*2;
FFTX(1)=FFTX(1)/2;
FFTX(length(FFTX))=FFTX(length(FFTX))/2;
FFTX=FFTX/length(x);
f=(0:NumUniquePts-1)*Fs/tnpts;

%*****************************************************************
% Plotting commands
%*****************************************************************

plot(f,FFTX);
l=axis;
axis([0 8 0 l(4)]);
xlabel('Wave Number (in)');
ylabel('Magnitude');
```

11. Picked points from graph for each mode. Example:

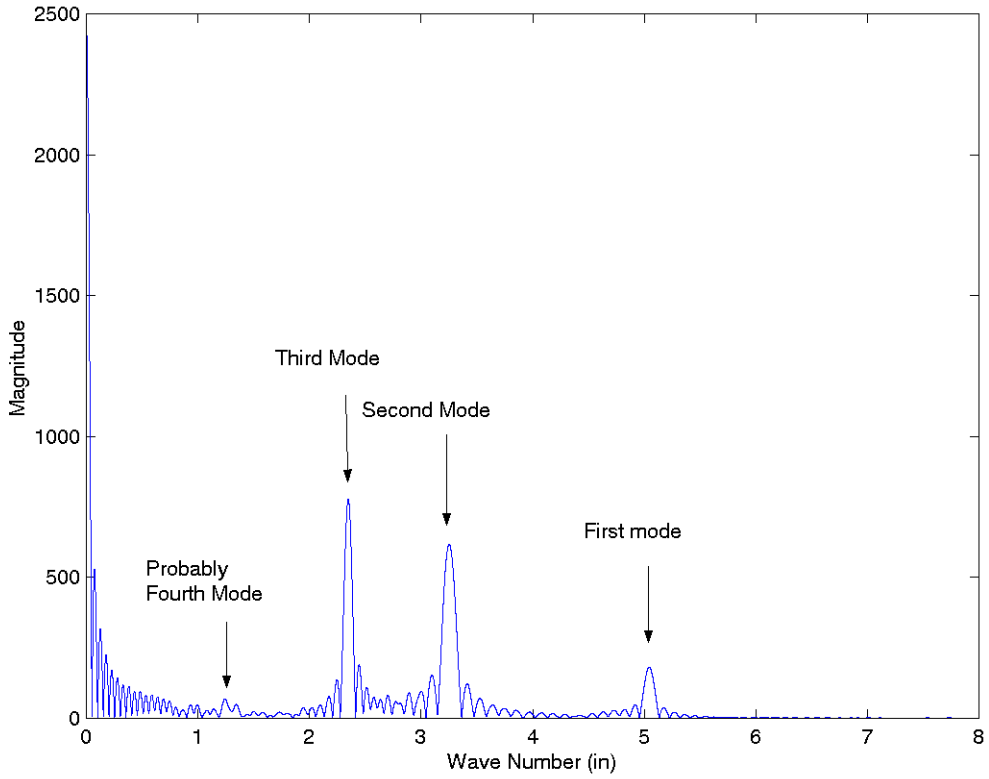

12. Calculated points on dispersion curve from frequency and wave numbers.

6.2 Broadband Dispersion Curves

1. Specified column of nodes and elements along axis of bar at the radius, in ABAQUS input file. Specified the stress data for specified nodes be written to output file, see example code.

```
*NSET,NSET=DATA, GENERATE
30,131230,82
*ELSET,ELSET=DATA, GENERATE
30,127950,80
.
.
*FILE OUTPUT, NUMBER INTERVAL=400
*EL FILE, ELSET=DATA
S
```

2. Converted output file for user post processing (at UNIX command prompt).

```
abaq5814 job=60x4800_sum800_40_45 convert=select
```

3. Coded Fortran file for data extraction.

```
****5****10***15***20***25***30***35***40***45***50***55***60***65***70***75
*  FORTRAN PROGRAM FOR COVERTING RESULTS FOR USE BY MATLAB
********************************************************************************

    PROGRAM RESULTS

    INCLUDE 'aba_param.inc'
    CHARACTER*80 FNAME
    REAL EL,STRESS
    DIMENSION ARRAY(513), JRRAY(NPRECD,513), LRUNIT(2,1)
    EQUIVALENCE (ARRAY(1),JRRAY(1,1))

    FNAME='60x4800_sum800_40_45'
    NRU=1
    LRUNIT(1,1)=8
    LRUNIT(2,1)=2
    LOUTF=0
    CALL INITPF(FNAME,NRU,LRUNIT,LOUTF)
    JUNIT=8
    CALL DBRNU(JUNIT)


    OPEN (UNIT=55, FILE="60x4800_sum800_40_45.txt", STATUS="UNKNOWN")

    DO 100 K1=1,100000000
      CALL DBFILE(0,ARRAY,JRCD)
      IF (JRCD.NE.0) GOTO 110
      KEY=JRRAY(1,2)
      IF (KEY.EQ.1) THEN
        EL=JRRAY(1,3)
      ELSEIF (KEY.EQ.11) THEN
        STRESS=ARRAY(4)
        WRITE (55,*) EL,STRESS
      END IF
 100       CONTINUE
 110       CONTINUE
    ENDFILE 55

    STOP
    END
```

4. Compiled Fortran file (at UNIX command prompt).

```
abaq5814 make job=60x4800_sum800_40_45
```

5. Executed Fortran file (at UNIX command prompt).

```
60x4800_sum800_40_45.x
```

6. Ran Matlab file to manipulate data and plot wave number spectrums.

```
%*****************************************************************
%                  FFT60x4800_SUM800_40_45.M
%*****************************************************************
% This program reads a text file of element and stress data.
% A Fourier Transform is performed on the data in the time domain
% and then in the space domain.  Dispersion curves are created.
%*****************************************************************
% Read data from file
%*****************************************************************

[element, s22]=textread('60x4800_sum800_40_45.txt','%f %f');

%*****************************************************************
% Put data into a matrix with stress for a given element in a
% given column with each row being a different time
%*****************************************************************

r=0;
for n=1:1:length(element)
  if round(element(n))==45
    r=r+1;
    results(r,round((element(n)-45)/480+1))=s22(n);
  else
    results(r,round((element(n)-45)/480+1))=s22(n);
  end
end

%*****************************************************************
% Perform DFT in time domain.
%*****************************************************************

[M,N]=size(results)

%NFFT=2.^(ceil((log(M))/log(2)))*8;
timefft=fft(results);
timeuniquepts=ceil((M+1)/2);

timefft=timefft(1:timeuniquepts,1:N);

mtimefft=abs(timefft);
mtimefft=mtimefft*2;

mtimefft(1,1:N)=mtimefft(1,1:N)/2;
mtimefft(timeuniquepts,1:N)=mtimefft(timeuniquepts,1:N)/2;
mtimefft=mtimefft/M;

freq=(0:timeuniquepts-1)*(401/1.0e-4)/(M);

%*****************************************************************
% Perform FFT in space domain with significant zero padding.
%*****************************************************************

NFFT=2.^(ceil(log(length(mtimefft(1,1:N)))/log(2)))*8;
spacefft=fft(mtimefft.',NFFT);

spaceuniquepts = ceil((NFFT+1)/2);
spacefft=spacefft(1:spaceuniquepts,1:timeuniquepts);

mspacefft=abs(spacefft);
mspacefft=mspacefft*2;
```

```
mspacefft(1,1:timeuniquepts)=spacefft(1,1:timeuniquepts)/2;
mspacefft(spaceuniquepts,1:timeuniquepts)=spacefft(spaceuniquepts,1:timeuniquepts)/2;
mspacefft=mspacefft/N;

lengthofbar=5;
numofsamples=300;
lengthofrun=2.25e-5;
numoftsamples=201;

k=(0:spaceuniquepts-1)*30/NFFT;

%****************************************************************
% Plot wave numbers for each frequency.
%****************************************************************

for j=1:2:81
    plot(k,mspacefft(1:spaceuniquepts,j));
    l=axis;
    axis([0 10 0 l(4)]);
    freqlabel = sprintf('frequency = %9.2f', freq(j));
    text(.5*10,.75*6,freqlabel);
    pause
end
```

7. Picked wave numbers from peaks for each frequency.
8. Calculated points on dispersion curves from frequency and wave number.

7. EXCEL FILES OF DATA POINTS FOR DISPERSION CURVES

If frequencies are omitted for a mode, then either the mode is not excited at that frequency or the wave number could not be determined.

7.1 Data for *20x6400* Dispersion Curves

Frequency (Hz)	k_1 (1/in.)	k_1*a/2*pi	c_1/c_0	k_2 (1/in.)	K_2*a/2*pi	c_2/c_0	k_3 (1/in.)	K_3*a/2*pi	c_3/c_0
303030.30	2.3047	0.5762	0.6438						
312500.00	2.4121	0.6030	0.6344	1.1914	0.2979	1.2844			
322580.65	2.5293	0.6323	0.6245	1.2793	0.3198	1.2347			
333333.33	2.6465	0.6616	0.6167	1.3574	0.3394	1.2025	0.2442	0.0611	6.6839
344827.59	2.7660	0.6915	0.6104	1.4352	0.3588	1.1765	0.3714	0.0929	4.5463
357142.86	2.8955	0.7239	0.6040	1.5149	0.3787	1.1544	0.4948	0.1237	3.5344
370370.37	3.0299	0.7575	0.5986	1.5968	0.3992	1.1358	0.6209	0.1552	2.9209
384615.38	3.1738	0.7935	0.5934	1.6797	0.4199	1.1212	0.7502	0.1876	2.5104
400000.00	3.3250	0.8313	0.5891	1.7773	0.4443	1.1020	0.8789	0.2197	2.2285
416666.67	3.4863	0.8716	0.5852	1.8750	0.4688	1.0881	1.0254	0.2564	1.9897
434782.61	3.6621	0.9155	0.5814	1.9922	0.4981	1.0687	1.1719	0.2930	1.8167
454545.45	3.8476	0.9619	0.5785	2.1150	0.5288	1.0524	1.3281	0.3320	1.6759
476190.48	4.0527	1.0132	0.5754	2.2656	0.5664	1.0292	1.5039	0.3760	1.5505
500000.00	4.2273	1.0568	0.5792	2.4414	0.6104	1.0028	1.6895	0.4224	1.4491
526315.79	4.5215	1.1304	0.5700	2.6660	0.6665	0.9667	1.9043	0.4761	1.3533
555555.56	4.7852	1.1963	0.5685	2.9492	0.7373	0.9224	2.1289	0.5322	1.2778
563380.28	4.8633	1.2158	0.5672	3.0330	0.7583	0.9096	2.1875	0.5469	1.2611
571428.57	4.9316	1.2329	0.5674	3.1162	0.7791	0.8979	2.2461	0.5615	1.2457
579710.14	5.0098	1.2525	0.5666	3.2129	0.8032	0.8835	2.3047	0.5762	1.2317
588235.29	5.0879	1.2720	0.5661	3.3050	0.8263	0.8715	2.3633	0.5908	1.2188
625000.00	5.4250	1.3563	0.5641	3.7210	0.9303	0.8225	2.6074	0.6519	1.1737
666666.67	5.8010	1.4503	0.5627	4.1990	1.0498	0.7774	2.8711	0.7178	1.1370
714285.71	6.2402	1.5601	0.5605	4.7168	1.1792	0.7415	3.1836	0.7959	1.0986
769230.77	6.7480	1.6870	0.5582	5.2930	1.3233	0.7116	3.5938	0.8985	1.0481
833333.33	7.3340	1.8335	0.5564	5.9430	1.4858	0.6866	4.1992	1.0498	0.9717
909090.91	8.0370	2.0093	0.5539	6.6840	1.6710	0.6660	5.0880	1.2720	0.8749

Frequency (Hz)	k_4 (1/in.)	K_4*a/2*pi	c_4/c_0
571428.57	0.9500	0.2375	2.9453
579710.14	1.1621	0.2905	2.4427
588235.29	1.3281	0.3320	2.1688
625000.00	1.8350	0.4588	1.6678
666666.67	2.2168	0.5542	1.4726
714285.71	2.5781	0.6445	1.3567
769230.77	2.9590	0.7398	1.2729
833333.33	3.3691	0.8423	1.2112
909090.91	3.8379	0.9595	1.1599

7.2 Data for *Over 30 Elements per Wavelength* Dispersion Curves

Freq. (Hz)	Element Config.	k_1 (1/in.)	k_1*a/2*pi	c_1/c_0	k_2 (1/in.)	K_2*a/2*pi	c_2/c_0
20000	4x5120	0.0977	0.0244	1.0024			
22222	5x3200	0.1075	0.0269	1.0122			
25000	5x3200	0.1221	0.0305	1.0026			
28571	5x3200	0.1416	0.0354	0.9880			
33333	5x3200	0.1660	0.0415	0.9833			
40000	5x3200	0.2002	0.0501	0.9783			
50000	5x3200	0.2490	0.0623	0.9833			
55556	8x2560	0.2734	0.0684	0.9950			
62500	8x2560	0.3125	0.0781	0.9793			
71429	8x2560	0.3515	0.0879	0.9950			
83333	8x2560	0.4141	0.1035	0.9854			
100000	12x3840	0.5039	0.1260	0.9717			
105263	12x3840	0.5273	0.1318	0.9775			
111111	12x3840	0.5625	0.1406	0.9672			
117647	12x3840	0.5977	0.1494	0.9638			
125000	12x3840	0.6328	0.1582	0.9673			
133333	12x3840	0.6797	0.1699	0.9605			
142857	12x3840	0.7383	0.1846	0.9475			
153846	12x3840	0.7969	0.1992	0.9453			
166667	12x3840	0.8789	0.2197	0.9286			
181818	12x3840	0.9727	0.2432	0.9153			
200000	12x3840	1.1130	0.2783	0.8799			
208333	12x3840	1.1836	0.2959	0.8619			
217391	12x3840	1.2656	0.3164	0.8411			
227273	12x3840	1.3711	0.3428	0.8117			
238095	12x3840	1.5000	0.3750	0.7772			
250000	16x5120	1.6484	0.4121	0.7426			
263158	16x5120	1.8203	0.4551	0.7079			
277778	16x5120	2.0078	0.5020	0.6774			
294118	16x5120	2.2030	0.5508	0.6537			
303030	20x6400	2.3047	0.5762	0.6438			
312500	20x6400	2.4121	0.6030	0.6344	1.1914	0.2979	1.2844
322581	20x6400	2.5293	0.6323	0.6245	1.2793	0.3198	1.2347
333333	20x6400	2.6465	0.6616	0.6167	1.3574	0.3394	1.2025
344828	24x1920	2.7618	0.6905	0.6114			
357143	24x1920				1.5109	0.3777	1.1575
370370	24x1920	3.0110	0.7528	0.6023	1.5974	0.3994	1.1353
384615	24x1920	3.1567	0.7892	0.5966	1.6776	0.4194	1.1226
400000	28x2240	3.3131	0.8283	0.5912	1.7752	0.4438	1.1033
416667	28x2240	3.4726	0.8682	0.5875	1.8718	0.4680	1.0900
434783	28x2240	3.6457	0.9114	0.5840	1.9859	0.4965	1.0720
454545	32x2560	3.8256	0.9564	0.5818	2.1066	0.5267	1.0566
476190	32x2560				2.2503	0.5626	1.0362
500000	32x2560	4.2602	1.0651	0.5747	2.4221	0.6055	1.0108
526316	36x2880	4.4939	1.1235	0.5735	2.6415	0.6604	0.9756
555556	36x2880	4.7458	1.1865	0.5732	2.9120	0.7280	0.9342
588235	40x3200	5.0444	1.2611	0.5710	3.2518	0.8130	0.8858

Freq. (Hz)	Element Config.	k_1 (1/in.)	k_1*a/2*pi	c_1/c_0	k_2 (1/in.)	K_2*a/2*pi	c_2/c_0
625000	45x3600	5.3677	1.3419	0.5702	3.6531	0.9133	0.8378
666667	45x3600	5.7347	1.4337	0.5692	4.1126	1.0282	0.7938
714286	50x4000	6.1535	1.5384	0.5684	4.6153	1.1538	0.7578
769231	60x4800	6.6355	1.6589	0.5676	5.1707	1.2927	0.7285

Freq. (Hz)	Element Config.	k_3 (1/in.)	K_3*a/2*pi	c_3/c_0	k_4 (1/in.)	K_4*a/2*pi	c_4/c_0
400000	28x2240	0.8784	0.2196	2.2298			
416667	28x2240	1.0267	0.2567	1.9872			
434783	28x2240	1.1700	0.2925	1.8196			
454545	32x2560	1.3226	0.3307	1.6829			
476190	32x2560	1.4958	0.3740	1.5589			
500000	32x2560	1.6853	0.4213	1.4527			
526316	36x2880	1.8902	0.4726	1.3634			
555556	36x2880	2.1165	0.5291	1.2853			
588235	40x3200	2.3471	0.5868	1.2272			
625000	45x3600	2.5873	0.6468	1.1829	1.8062	0.4516	1.6944
666667	45x3600	2.8499	0.7125	1.1455	2.1930	0.5483	1.4886
714286	50x4000	3.1498	0.7875	1.1104			
769231	60x4800	3.5229	0.8807	1.0692	2.9160	0.7290	1.2917

7.3 Data for *Broadband* Dispersion Curves

Frequency (Hz)	k_1 (1/in.)	k_1*a/2*pi	c_1/c_0	k_2 (1/in.)	K_2*a/2*pi	c_2/c_0	k_3 (1/in.)	K_3*a/2*pi	c_3/c_0
40000	0.1868	0.0467	1.0577						
60000	0.2893	0.0723	1.0245						
80000	0.3918	0.0980	1.0086						
100000	0.4944	0.1236	0.9991						
120000	0.5969	0.1492	0.9931						
140000	0.7068	0.1767	0.9784						
160000	0.8240	0.2060	0.9591						
180000	0.9448	0.2362	0.9411						
200000	1.0877	0.2719	0.9083						
220000	1.2598	0.3150	0.8626						
240000	1.4760	0.3690	0.8032						
260000	1.7432	0.4358	0.7367						
280000	1.9958	0.4990	0.6930						
300000	2.2450	0.5613	0.6601						
320000	2.4210	0.6053	0.6529	1.1940	0.2985	1.3239			
340000	2.6880	0.6720	0.6248	1.3770	0.3443	1.2197			
360000	2.8895	0.7224	0.6154	1.5125	0.3781	1.1757	0.4835	0.1209	3.6779
380000	3.0945	0.7736	0.6066	1.6405	0.4101	1.1442	0.6920	0.1730	2.7125
400000	3.2850	0.8213	0.6015	1.7575	0.4394	1.1242	0.8770	0.2193	2.2530
420000	3.4860	0.8715	0.5951	1.8787	0.4697	1.1043	1.0255	0.2564	2.0231
440000	3.6841	0.9210	0.5899	2.0020	0.5005	1.0856	1.1830	0.2958	1.8372

Frequency (Hz)	k_1 (1/in.)	k_1*a/2*pi	c_1/c_0	k_2 (1/in.)	K_2*a/2*pi	c_2/c_0	k_3 (1/in.)	K_3*a/2*pi	c_3/c_0
460000	3.8820	0.9705	0.5853	2.1277	0.5319	1.0679	1.3404	0.3351	1.6952
480000	4.0485*	1.0121	0.5857	2.2560	0.5640	1.0510	1.5050	0.3763	1.5754
500000	4.2350*	1.0588	0.5832	2.3950	0.5988	1.0312	1.6480	0.4120	1.4987
520000	4.3980	1.0995	0.5840	2.5525	0.6381	1.0063	1.8130	0.4533	1.4168
540000	4.5980*	1.1495	0.5801	2.7360	0.6840	0.9749	1.9740	0.4935	1.3513
560000	4.7560	1.1890	0.5816	2.9298	0.7325	0.9442	2.1314	0.5329	1.2978
580000	4.9560*	1.2390	0.5781	3.1494	0.7874	0.9097	2.2778	0.5695	1.2578
600000	5.1350*	1.2838	0.5772	3.3582	0.8396	0.8825	2.4150	0.6038	1.2272
620000	5.3150*	1.3288	0.5762	3.5780	0.8945	0.8559	2.5450	0.6363	1.2034
640000	5.4860*	1.3715	0.5763	3.7975	0.9494	0.8325	2.6770	0.6693	1.1809
660000	5.6650*	1.4163	0.5755	4.0190	1.0048	0.8112	2.7940	0.6985	1.1668
680000	5.8450*	1.4613	0.5747	4.2225	1.0556	0.7955	2.9225	0.7306	1.1493
700000	6.0260*	1.5065	0.5738	4.4385	1.1096	0.7790	3.0580	0.7645	1.1307
720000	6.1950*	1.5488	0.5741	4.6360	1.1590	0.7672	3.1824	0.7956	1.1176
740000	6.3830	1.5958	0.5727	4.8600	1.2150	0.7521	3.3215	0.8304	1.1005
760000	6.5480	1.6370	0.5733	5.0755	1.2689	0.7397	3.4610	0.8653	1.0847
780000	6.7420	1.6855	0.5715	5.2808	1.3202	0.7296	3.6150	0.9038	1.0658
800000				5.4750	1.3688	0.7218	3.7760	0.9440	1.0465

Frequency (Hz)	k_4 (1/in.)	K_4*a/2*pi	c_4/c_0
580000	1.2820**	0.3205	2.2348
600000	1.4840**	0.3710	1.9971
620000	1.7250**	0.4313	1.7754
640000	1.9461**	0.4865	1.6245
660000	2.1130**	0.5283	1.5429
680000	2.2780†	0.5695	1.4745
700000	2.4320†	0.6080	1.4218
720000	2.5850†	0.6463	1.3758
740000	2.7210†	0.6803	1.3434
760000	2.8530†	0.7133	1.3158
780000	2.9810†	0.7453	1.2925
800000	3.1128†	0.7782	1.2695

The majority of the wavenumbers were determined from a set of data points located at 0.75 the radius. The marked wavenumbers (see below) indicate the data was taken from a different location on the radius.

*	$0.25 \cdot radius$
**	$0.5 \cdot radius$
†	$1.0 \cdot radius$ (surface)

Los Alamos
NATIONAL LABORATORY
Los Alamos, New Mexico 87545